NASA TECHNICAL MEMORANDUM

NASA TM X-1733

NASA TM X-1733

DESIGN AND PERFORMANCE OF A FLUERIC SHOCK POSITION SENSOR FOR A MIXED-COMPRESSION SUPERSONIC INLET

by William S. Griffin

Lewis Research Center

Cleveland, Ohio

NATIONAL AERONAUTICS AND SPACE ADMINISTRATION • WASHINGTON, D. C. • JANUARY 1969

NASA TM X-1733

DESIGN AND PERFORMANCE OF A FLUERIC SHOCK POSITION SENSOR FOR A MIXED-COMPRESSION SUPERSONIC INLET

By William S. Griffin

Lewis Research Center
Cleveland, Ohio

NATIONAL AERONAUTICS AND SPACE ADMINISTRATION

For sale by the Clearinghouse for Federal Scientific and Technical Information
Springfield, Virginia 22151 – CFSTI price $3.00

ABSTRACT

A flueric sensor for normal shock position has been developed and tested on a Mach 2.5 mixed-compression axisymmetric supersonic inlet. The sensor detects shock position by sensing the most rearward minimum in static wall pressure profile. Static and dynamic responses of the sensor were evaluated. Static response agreed relatively well with theory, but dynamic response indicated further improvements to the sensor are necessary. Design approaches and fluid jet amplifier and component data are included as well as suggestions for improving the sensor's dynamic performance.

CONTENTS

DESIGN AND PERFORMANCE OF A FLUERIC SHOCK POSITION SENSOR FOR A MIXED-COMPRESSION SUPERSONIC INLET

by William S. Griffin

Lewis Research Center

SUMMARY

As a result of the requirements of control loops for advanced supersonic inlets, a program has been initiated at Lewis Research Center to develop a sensor for normal shock position in a mixed-compression inlet. Fluid jet amplifiers were chosen as the sensor's operating elements because of their potential advantages in a flight-weight application. A prototype flueric circuit was developed and tested on a Mach 2.5 supersonic inlet. The circuit detects the shock position by sensing the most rearward minimum in the static wall pressure profile.

Both static and dynamic tests were performed in the wind tunnel and compared with bench tests. In general, the static performance of the sensor was satisfactory and agree with bench test results. Erratic operation of the sensor was observed when the shock was in the vicinity of the aft throat boundary layer bleeds. This is believed to be due to a combination of high noise in the signals furnished to the sensor when the shock is in this location and an excessive dynamic sensitivity of the sensor to such noise. Dynamic tests indicated that full-amplitude response of the sensor could be obtained for full amplitudes of shock motion and shock cyclic frequencies in excess of 50 hertz. At reduced amplitudes of shock motion, the response of the sensor was much lower, however. This is ascribed to the previously mentioned dynamic sensitivity. Corrections are suggested which should improve the sensor's performance in this regard.

Design approaches and fluid jet amplifier component data are presented to permit other researchers to design duplicate or improved versions of the sensor described herein.

INTRODUCTION

For supersonic inlets which have a high degree of internal contraction, refined control systems are required to maintain inlet pressure and flow recoveries at optimum

levels while, at the same time, preventing the internal normal shock wave from being expelled out the front of the inlet (inlet unstart). The optimum conditions of pressure recovery and bleed flow in general allow only a small stability margin relative to such inlet unstart. Most current control concepts use throat exit pressure or pressure ratio (Mach number downstream of the internal shock) as the sensed parameter, and by manipulating the downstream bypass doors indirectly keep the inlet close to the best operating conditions with satisfactory stability margin. Variations and uncertainties in this setting due to changes in flight speed and altitude and variations in inlet geometry, due for example to aerodynamic loading and thermal growth, complicate such a control scheme and may require increased stability margin and decreased performance. An alternate and more direct control concept would use normal shock position itself as the sensed parameter. Stability margin would be thus directly controlled and optimum operation more easily maintained.

Development of a reliable normal shock wave position sensor has been a difficult task for inlets which have a high degree of internal contraction. The irregular, nonideal flow patterns found in an operational inlet render useless many schemes which would

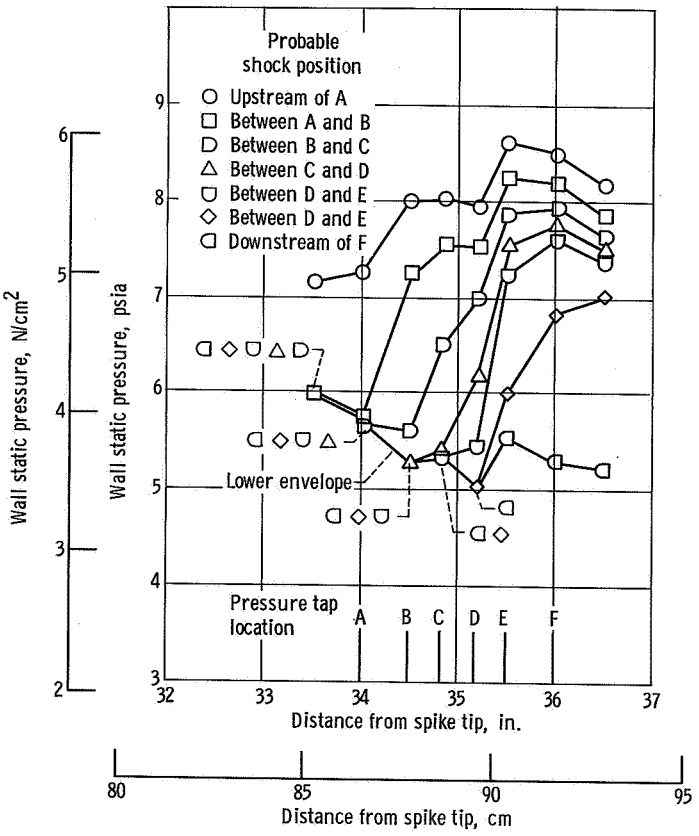

Figure 1. - Typical wall static pressure distributions as function of shock position.

work with ideal flow patterns. As an example of the wall pressure distributions which might be expected in the vicinity of the shock wave, figure 1 shows data taken from a Mach 2.5 supersonic inlet which was tested in the 10 by 10 foot supersonic wind tunnel at Lewis Research Center. The inlet is a 25-inch (63-cm) diameter, axisymmetric mixed-compression inlet with a translating centerbody (ref. 1). The data plotted in figure 1 were taken at zero angle of attack. The wall pressures shown in figure 1 are far from ideal. Upstream of the shock wave small variations in static wall pressure occur as a result of imperfectly cancelled oblique shock compression waves which have passed through the throat at pressure tap D a dip occurs which is caused by a set of boundary layer bleeds. Thus, detection of the shock by simply measuring the presence of a positive wall pressure gradient is not likely to be successful. Alternatively, determining the shock position by measuring the absolute values in wall static pressure levels is made difficult by the fact that these levels change both as the total pressure of the flow entering the inlet changes and also as the geometry of the inlet changes. A flight type inlet would have decidedly poorer pressure distributions due to factors such as larger fabrication tolerances. Pressure distribution will also vary with angle of attack.

A program was instituted at Lewis to develop a more reliable normal shock wave position sensor. After studying several schemes, it was decided that the best method of directly determining shock wave position would be by digital comparison of a series of static wall pressure tap readings. Both electronic and flueric implementations of the sensing scheme were made.

A flueric shock position sensor composed of digital fluid jet amplifiers appeared to have a number of advantages for potential flight-weight applications. Since there are no moving parts, its wear rate should be low and its reliability high. Operational speeds of the component amplifiers are fast in comparison to most of the inlet's characteristic time constants and to the speeds of the bypass doors. Since fluerics can be packaged into relatively small integrated assemblies and would use the flow in the duct as a power source, it should be possible to make a completely self-contained sensor which could be located in the inlet cowl. A variety of outputs could be obtained from the sensor such as a series of on-off pressure actuated switches or the displacement of a bellows. If desired, the sensor's outputs could be used directly as a signal input to the bypass door actuators, thus obviating the necessity of running electrical lines back to the central electronics in the aircraft's fuselage.

This report describes the design and testing of such a flueric shock position sensor. Design approaches and techniques are discussed. The aim herein is to provide a basis for the design of other more advanced flueric shock position sensors and to illustrate some of the practical advantages and shortcomings of the present sensor.

DESIGN APPROACHES

Criteria for Establishing Shock Wave Position

It can be seen, by referring to figure 1, that the shock wave position may be estimated reasonably well by eye. The visual criteria for establishing this position are the presence of a strong positive pressure gradient preceded by either a neutral or slightly negative pressure gradient. The strong pressure gradient exists over several pressure taps. Since it would be desirable to specify the shock wave position to a resolution of one pressure tap spacing, the effective position of the shock wave may be defined as the intersection of the best straight line average of the neutral pressure gradient curve with that of the positive gradient curve. To the left of this intersection, the flow would presumably be undisturbed, while to the right of it, the pressure rises associated with the normal shock would begin to appear. Thus, for example, the shock position represented by the symbol $\square$ in figure 1 would be somewhere between pressure taps B and C: For the shock position represented by the symbol $\diamond$, the shock would be between taps D and E.

These criteria may be put into mathematical form. To simplify the logical equations and, hence, the required flueric circuitry, only three pressure taps are compared at a time as opposed to the five or six that the eye might compare. The logical equations for pressure profile minimums which represent possible shock locations can thus be written:

$$\left.\begin{aligned} S_{EF} &= (D \geq E) \cdot (E < F) \\ S_{DE} &= (C \geq D) \cdot (D < E) \\ S_{CD} &= (B \geq C) \cdot (C < D) \\ S_{BC} &= (A \geq B) \cdot (B < C) \\ S_{AB} &= (A < B) \end{aligned}\right\} \qquad (1)$$

where the symbol $\cdot$ denotes the Boolean logical AND function.

The use of only three pressure tap readings precludes the averaging of a series of readings to establish a trend in the gradient. Thus, the irregularities in the supersonic flow wall pressure distribution (lower bound of the curves in fig. 1) might cause false indications of shock wave position. Fortunately, this difficulty may be overcome. It is

noted that the wall pressure curves do not have many irregularities downstream of the shock wave. The only one which exists is a dip caused by a wall boundary layer bleed (located at pressure tap D). This dip, however, is not prominent until the static wall pressure has risen well above its value for supersonic flow conditions. Examples would be the curves represented by circles or squares. Thus, if a method can be found to bias out a reading of shock position when the average wall pressures near this position are much higher than supersonic values, a shock wave position may be simply defined as being at the farthest aft location of indicated pressure profile minimums. As will be shown later, the biasing out process is taken care of automatically by the fluid jet amplifiers. Given this property of the fluid amplifiers, the logical equations necessary for determining effective shock position are

$$\left.\begin{aligned} S'_{EF} &= (D \geq E) \cdot (E < F) \\ S'_{DE} &= (C \geq D) \cdot (D < E) \cdot \overline{S}'_{EF} \\ S'_{CD} &= (B \geq C) \cdot (C < D) \cdot \overline{S}'_{DE} \cdot \overline{S}'_{EF} \\ S'_{BC} &= (A \geq B) \cdot (B < C) \cdot \overline{S}'_{CD} \cdot \overline{S}'_{DE} \cdot \overline{S}'_{EF} \\ S'_{AB} &= (A < B) \cdot \overline{S}'_{BC} \cdot \overline{S}'_{CD} \cdot \overline{S}'_{DE} \cdot \overline{S}'_{EF} \end{aligned}\right\} \qquad (2)$$

where S'_{EF} denotes a shock between pressure taps E and F, S'_{DE} denotes a shock between pressure taps D and E, etc., and the symbol $\overline{\ }$ denotes the Boolean logical negation.

In a practical control system, the output signals of the shock position sensor would probably be converted into a stepwise proportional signal suitable for driving a proportional control element. Thus, the preceding logical equations, although correct, should be rewritten to give such a signal. Double primes are used to denote the new signals. Such a stepwise proportional output would use the output S_{AB} to denote a shock position between stations A and B, the presence and sum of outputs S_{AB} and S_{BC} to denote a shock between stations B and C, and so on, where the unprimed S's are the pressure gradient changes defined in equation (1). Mathematically, the new criteria may be expressed as

$$
\left.
\begin{aligned}
S''_{EF} &= (D \geq E) \cdot (E < F) \\
S''_{DE} &= (C \geq D) \cdot (D < E) + S''_{EF} \\
S''_{CD} &= (B \geq C) \cdot (C < D) + S''_{DE} + S''_{EF} \\
S''_{BC} &= (A \geq B) \cdot (B < C) + S''_{CD} + S''_{DE} + S''_{EF} \\
S''_{AB} &= (A < B) + S''_{BC} + S''_{CD} + S''_{DE} + S''_{EF}
\end{aligned}
\right\} \qquad (3)
$$

where, in addition to the previously defined logical quantities, + denotes the Boolean logical OR function. Thus, in equation (3), if a possible shock location or pressure profile minimum existed between taps B and C ($S_{BC} = (A \geq B) \cdot (B < C)$ exists) the outputs S''_{BC} and S''_{AB} would result. Similarly, if a pressure profile minimum between taps C and D was detected ($S_{CD} = (B \geq C) \cdot (C < D)$ exists), equation (3) would yield the three outputs S''_{CD}, S''_{BC}, and S''_{AB}. Thus, as the farthest right indicated shock position advances to the right (downstream of the throat), more and more outputs appear in equation (3). Their weighted sum would thus constitute a stepwise proportional indication of normal shock wave position. It should be noted that if a pressure profile minimum yields an indicated shock position, for example, S''_{DE}, other pressure profile minimums to the left of it, for example, S_{AB} or S_{BC}, are of no consequence since the double primed outputs S''_{AB} and S''_{BC} are already triggered by existence of the downstream output S''_{DE}.

Flueric Circuitry Design

Equations (3) were used as the basis of design for a fluid jet amplifier shock position sensor. The sensor's block diagram is shown in figure 2. Functionally, the sensor is divided into three main parts. The first part consists of a series of comparators which determine which of two adjacent wall tap pressures is the larger. The outputs of the comparator unit are in logically complementing pairs. Thus, if the output $A \geq B$ exists, the output $A < B$ must not exist.

The second portion of the sensor consists of a series of logical AND units. These AND units compare adjacent comparator output signals and issue outputs only when the two adjacent comparator signals exist (have the logical value of true). Thus, the output S_{BC} exists only when the comparator outputs $A \geq B$ and $B < C$ simultaneously exist.

The third portion of the sensor is an output stage which provides strong output signals which are stepwise proportional to the most rearward indicated shock position. Thus, if

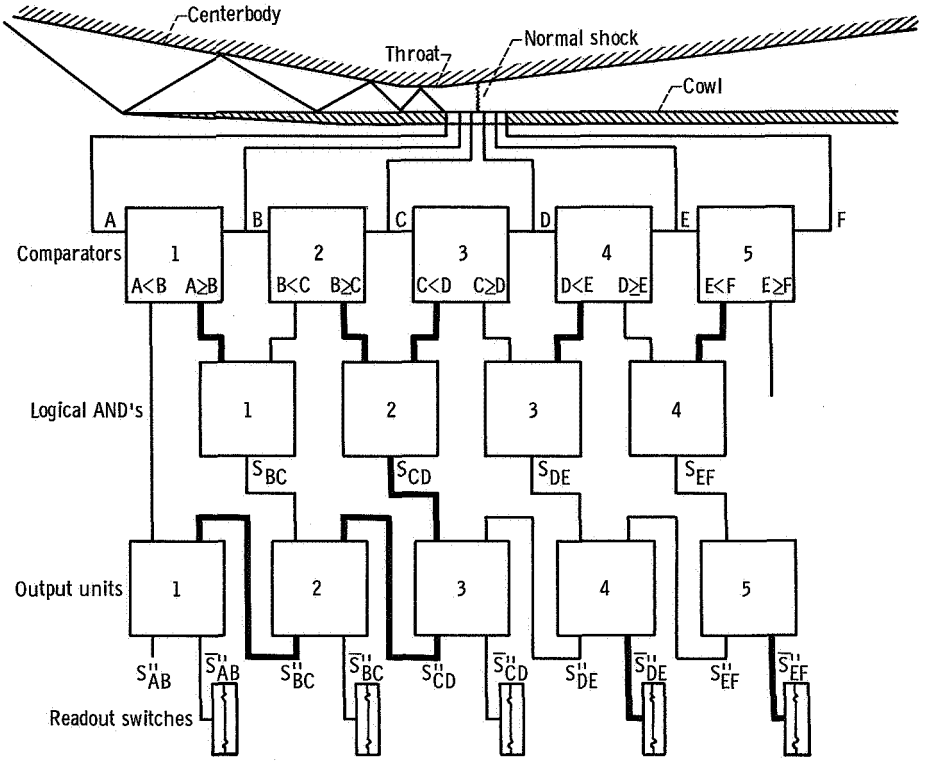

Figure 2. - Block diagram of shock position sensor.

the AND unit signal S_{CD} exists, the output unit will generate the signals S''_{AB}, S''_{BC}, and S''_{CD}. The heavy lines in figure 2 indicate the outputs that are activated when the shock is between C and D.

Figure 3 shows a schematic of the flueric shock position sensor with the three main functional blocks labeled. The symbology is that used in reference 2. The top row of comparator units are conventional fluid jet amplifier OR-NOR units. Their control ports are driven in parallel and the OR-NOR units are used as monostable comparators. In combination with the opposite side vent V_1 (shown by two parallel dotted lines), they provide a differential pressure signal to the amplifier. Thus, with the example of comparator 2, an output will exist in the amplifier's R_2 leg if $B \geq C$ and will exist in the R_1 leg of the amplifier if $C > B$. Since a differential pressure is applied to the control ports of the comparator amplifiers, they will not be switched by changes in average pressure level but by differences in pressures indicating pressure gradients. Thus, even if the inlet's internal flow conditions are not on design, the comparator amplifiers will still perform their task of comparing pressures.

The second row of units are the logical AND units and are also composed of conventional OR-NOR type fluid jet amplifiers. Again, both control ports are driven in parallel.

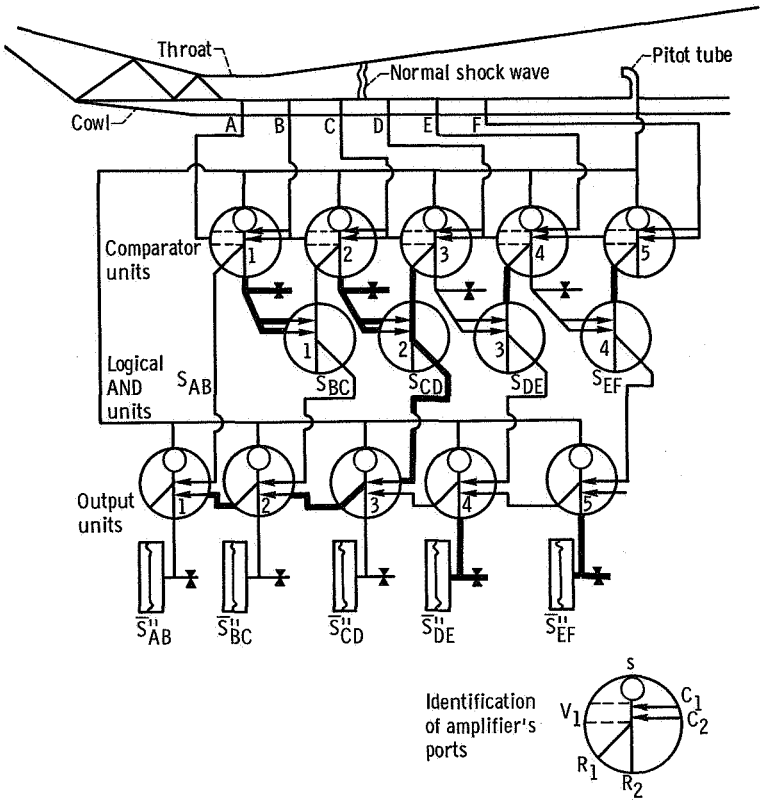

Figure 3. - Schematic of flueric shock position sensor.

The logical AND function is obtained by supplying one input signal to the power nozzle and the other signal to the control port. The power stream jet is directed out the R_1 leg of the amplifier and the logical product (AND) of the two applied signals is thus obtained. If either the power nozzle signal or the control port signal is applied separately, there will be no output from the R_1 (AND) leg.

The outputs of the logical AND units are fed into the control ports of the fluid jet amplifiers on the output units. The output units are also OR-NOR units used conventionally. The fluid jet amplifiers of the output unit are interconnected such that if one amplifier is made to switch by a signal from the AND unit, all other output fluid jet amplifiers that represent shock positions upstream of it will be switched. Thus, if the logical AND unit A2 is activated creating an output signal S_{CD}, the output unit 3 will be activated. Its "OR" output will activate output unit 2 which will, in turn, activate unit 1. Inspection of the circuit will show that the logical equations (3) are satisfied. The heavy signal lines in figure 3 indicate the outputs that are activated when the shock is between C and D.

Pressure actuated switches were used to read the outputs of the output unit fluid jet amplifiers. The switches were connected to the logical NOR legs of the amplifiers to avoid long charging time constants in the carry signal lines between amplifiers. Supply

flow to the circuit is furnished by a total pressure probe immersed in the inlet's main flow. Thus, supply flow to the circuit is furnished as long as the inlet is operating. Not shown is an enclosure around the sensor which provides a common atmosphere to the exhaust ports of the fluid jet amplifiers. The collected exhaust is then dumped to ambient by means of a choked orifice. Exhaust ports on the amplifier, which dump into the enclosure, are not shown but are understood to exist (ref. 2).

The total system exhaust flow is composed of the comparator and output amplifier power nozzle flows and the comparator amplifiers' control port flows. The power nozzle flows are approximately constant, since the power nozzles are operating very close to choked conditions. Control flows to the comparator amplifiers will vary as a function of shock wave position, but are usually less than 20 percent of the power nozzle flows. Thus, the exhaust flows of the amplifiers will be approximately constant plus or minus a small amount as a result of shock wave movement. Sensor exhaust pressure, which is proportional to the exhaust flow of the fluid jet amplifiers, will also be constant plus or minus a small amount (approximately 10 percent) as a result of shock wave movement.

Since the power nozzle and control flows of the sensor's fluid jet amplifiers will vary directly with the total pressure of the inlet's internal flow, their exhaust flow and, hence, the sensor exhaust pressure will also vary directly with the inlet's total pressure. Thus, sensor exhaust pressure will always be a given fraction of inlet total pressure, plus or minus a small deviation as a result of shock wave movement. This useful property is utilized to bias out the boundary layer induced dip in wall pressure at pressure tap D.

Biasing Out Bleed Induced Dips in Wall Static Pressure

It is seen by again referring to figure 1 that a systematic dip in the wall static pressures occurs at pressure tap D. This dip in wall pressure is caused by the presence of a boundary layer bleed located at pressure tap D. For the curves composed of circles or squares, the dip could be read as the presence of a throat normal shock. Since the sensor is designed to indicate the most rearward sensed shock position as being the actual one, such an error could be serious. For the case of the curve composed of circles, the normal shock is as far forward in the throat as it can go without causing inlet unstart. Thus, if the shock position sensor misread the curve composed of circles as indicating a shock position at pressure tap D, the bypass doors might be commanded to close and thus unstart the inlet.

One method of eliminating such an error in indicated shock position is to make use of the fact that, once the shock has advanced past pressure tap D, the bleed induced dip is not apparent until the wall static pressure has risen well above its supersonic value. Thus, if the comparator elements of the flueric shock position sensor can be made sensitive to gradients in wall static pressure only when their value is close to supersonic

flow conditions, the boundary layer bleed induced dip in wall static pressure will not cause a false shock position to be indicated.

Fortunately, this property of variable switching sensitivity is an inherent characteristic of the OR-NOR units used in the flueric shock position sensor. Figure 4 shows a plot of average control port pressure required to switch an OR-NOR unit to and from its R_1 receiver (forward and reverse switch in the figure) as a function of the vent V_1 pressure. Both the control port and the vent V_1 pressures are gage pressures and are normalized with respect to the OR-NOR unit's gage supply pressure.

As can be seen from the figure, if the vent V_1 pressure is close to ambient, the switching sensitivity of the OR-NOR unit is high. An average control port pressure of only 5 percent of supply will switch it. However, if the vent V_1 pressure is raised, the switching sensitivity of the OR-NOR unit is markedly decreased. For a normalized vent V_1 pressure of 40 percent of supply, the normalized control port pressure required to forward switch the OR-NOR unit is 79 percent. The differential pressure required to

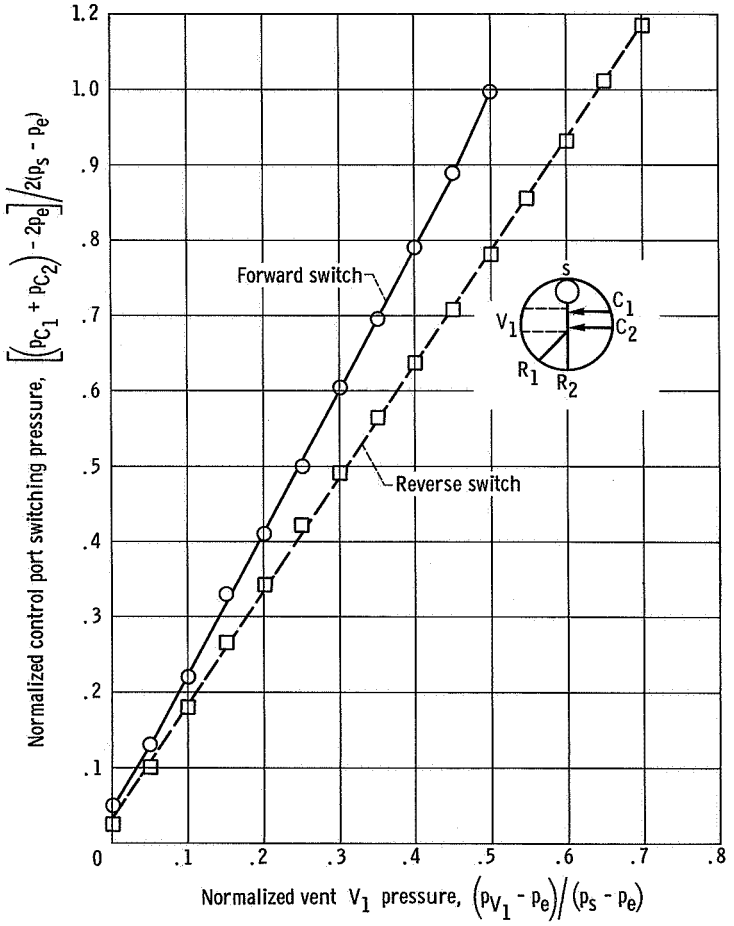

Figure 4. - Control port forward and reverse switching pressures as function of vent V_1 pressure.

forward switch the unit is therefore 39 percent (79 percent-40 percent) of supply pressure. Thus, the differential pressure required to switch the OR-NOR unit has risen from 5 percent of supply to 39 percent of supply for a vent V_1 pressure rise from 0 percent of supply to 40 percent of supply. This constitutes the desired decrease the switching sensitivity as a result of elevated signal (control port and vent V_1) pressures. All that is required for this property to be usefully utilized in the flueric shock position sensor is for the sensor's exhaust pressure to remain fairly close to the inlet throat static wall pressure for supersonic flow conditions.

Since, as mentioned previously, the sensor exhaust pressure remains a relatively fixed fraction of inlet total pressure, nominal sensor exhaust pressure may be set equal to nominal inlet throat supersonic flow pressures. The shock position sensor's comparator amplifiers will be easy to switch at the front of the shock wave but hard to switch once the shock wave has passed. Thus, the required biasing out of the boundary layer bleed induced dip in subsonic wall pressure profile is automatically provided.

This inherent method of biasing out the effects of the boundary layer induced dip in wall static pressure will work only as long as the inlet throat static pressure is a reasonably constant fraction (say within ±10 percent) of the inlet throat total pressure. Normally, with a properly functioning throat area control loop, this will be the case. Malfunctions of the throat area control loop or constraints on inlet operation as a result of operating envelope and engine limitations could cause the average local throat static pressure to vary from the design value, however. For such situations, a pressure tap could be placed ahead of the most forward expected shock position. The output of this pressure tap could be the reference (tangential) pressure for a vortex valve through which the sensor's exhaust flow would be passed. The vortex valve would regulate sensor exhaust pressure and hold it equal to the reference tap pressure. Thus, sensor exhaust pressure could still be maintained equal to the inlet's wall static pressure upstream of the shock.

BREADBOARD SHOCK POSITION SENSOR

A preliminary breadboard model was made of the previously described circuit. Commercially available Corning OR-NOR fluid jet amplifiers equipped with barbed fittings were used and interconnected with thermoplastic tubing. Figure 5 shows a typical amplifier as received and gives some nominal operating characteristics. Performance curves of control port and receiver pressure-flow characteristics are given in appendix B. No manifolding was placed around the exhaust ports of the amplifiers, laboratory ambient served as exhaust pressure, and supply pressures to the amplifiers were maintained at 10.0 psig (6.9 N/cm^2). The interconnection lines were sized using

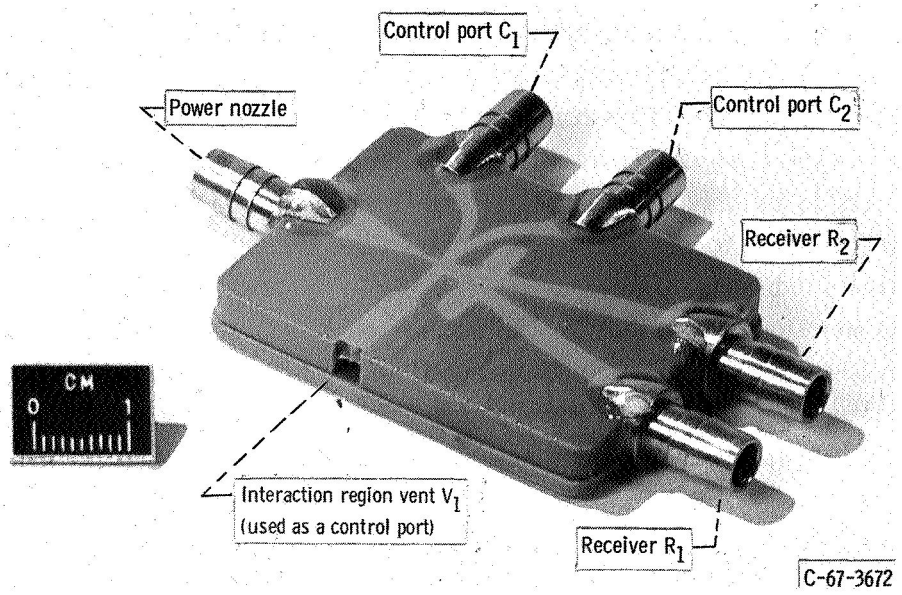

Figure 5. - Digital OR-NOR fluid jet amplifier used in breadboard and prototype shock position sensors Power nozzle size, 0.020 by 0.080 inch (0.0508 by 0.203 cm); minimum operational Reynolds number, 2340 (estimated); maximum operational Mach number, 1.2 (estimated).

single reflection termination (ref. 5), and pressure actuated diaphragm switches were used as the readout devices.

Bench tests were made of the circuit to check speeds of response, logical operation, and occurrence of timing hazards (interference of pulses as a result of two amplifiers switching simultaneously). Individual amplifiers exhibited the expected 0.0005-second switching times and timing hazards did not prove a problem for circuit operating speeds of 160 hertz or lower. As a result of these favorable preliminary results, it was decided to make a prototype model which would be suitable for testing on a NASA Mach 2.5 research inlet. Primary motivations for constructing the prototype sensor were the following:

(1) To gain experience with fluid jet amplifier operation under environments typical of a supersonic inlet

(2) To gain experience in packaging amplifiers into a closed system in which the exhaust passages would be restricted

(3) To evaluate problems that would be peculiar to an operational sensor mounted on an inlet and which would not be present in a laboratory bench test

(4) To attempt to establish the operational practicality of a flueric shock position sensor

Scaling of Amplifier Size and Operating Pressure

The physical size of the internal geometry of the fluid jet amplifiers and their operating pressures cannot be chosen arbitrarily, but must be compatible with two bounds on the amplifiers' operation. These bounds are (1) a lower power nozzle Reynold's number, and (2) an upper power nozzle Mach number. These two limits can be in conflict with each other. For example, if the power nozzle throat velocity is increased in order to raise the power nozzle Reynold's number, the maximum power nozzle Mach number may be exceeded. This situation becomes worse as the average absolute pressure level in the fluid jet amplifier is lowered or the absolute temperature of the supply gas is increased. For a given supply gas total temperature, the lowest exhaust pressure at which a digital fluid jet amplifier can operate occurs when the maximum throat Mach number and the minimum throat Reynold's number are simultaneously reached. If it is desired to use a digital fluid jet amplifier of given geometry at a lower amplifier exhaust pressure or at a higher supply gas temperature, the only alternative left is to increase the physical dimensions of the amplifier. Thus, for a given supply gas total temperature, the minimum amplifier size that can be used varies inversely with the amplifier's exhaust pressure. Details of the scaling procedures and choices made in determining the amplifier size that was used in the sensor are covered in appendix A. A sensor fabricated of the selected fluid jet amplifiers should be capable of operating in an SST inlet at 70 000 feet (standard atmosphere) at a free stream Mach number of 2.7.

Interconnection of Elements

To minimize the effect of reflected waves, either acoustical termination or single reflection termination was used to size all lines. Acoustical termination occurs when the load at the end of a line is equal to the line's surge impedance. Under such conditions, a pulse sent down the line is completely absorbed and no reflections are sent back toward the source which drives the line. Single reflection termination occurs when the average output impedance of the source is approximately equal to the surge impedance of the line while the load's impedance is very much greater (details of this method of termination are given in ref. 5). If the source sends a pulse down the line, it will be partially reflected by the load. The reflected pulse, however, is completely absorbed by the output impedance of the source. Since the reflected pulse is not seen as a separate pulse by the load, the pulse delivered to the load appears indistinguishable from that delivered by an acoustically terminated line. Because of the larger line diameter of the single reflection line, frictional losses in it will be much lower than in an acoustically terminated line. Hence, to minimize frictional losses, single reflection termination was used

unless the lines were very short. Details of the sizing procedures are not included since they are adequately covered in reference 3. So that the choice of line sizes used may be verified the pressure-flow characteristics of the control ports, vent V_1, and receivers of an OR-NOR type fluid jet amplifier are presented in appendix B.

In obtaining the control port pressure-flow characteristics of the sensor's component amplifiers, it was discovered that the switching performance of the amplifiers was very sensitive to variations in the interaction region vent V_1 pressure (shown as a pair of dotted lines, top row of elements, fig. 3). In particular, if the interaction region vent V_1 pressure was lowered below ambient more than 1 or 2 percent of the difference between the amplifier's supply and exhaust pressures, the amplifier would not switch back to its NOR leg. Thus, when the case of output unit S''_{BC} of figure 3 is considered, if no control signal were furnished to it by the logical AND unit and at the same time its interaction region vent V_1 pressure was slightly subambient, it would still remain switched, just as if a signal from the logical AND unit had never been removed. This problem is discussed in more detail in appendix B and points out a potential hazard that accompanies the use of these fluid jet amplifier OR-NOR units.

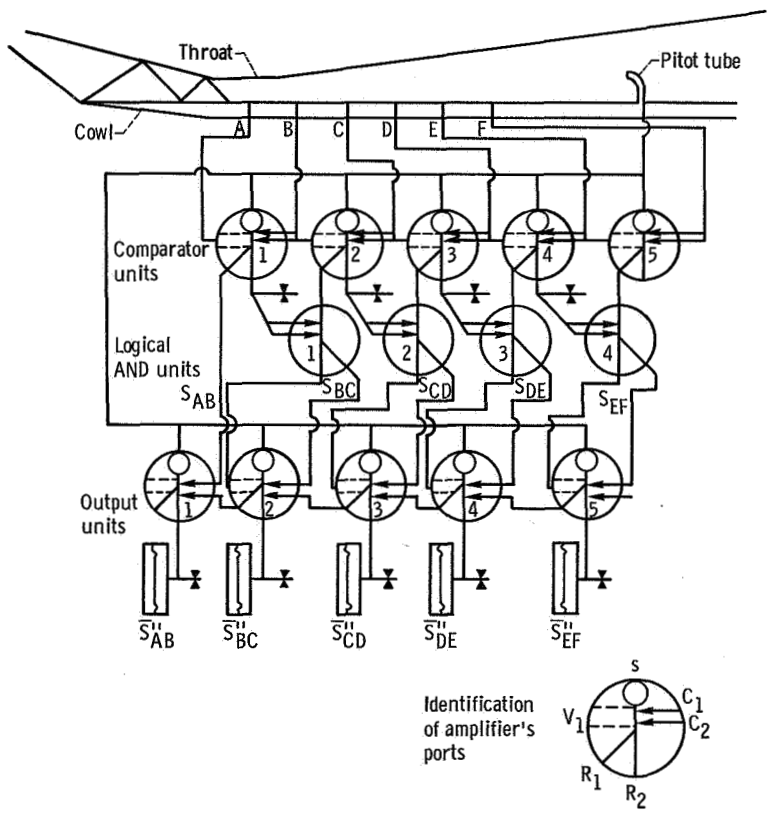

Figure 6. - Schematic of flueric shock position sensor.

A partial remedy to this problem was effected by connecting the interaction region vents of the output units to the NOR leg of the OR-NOR fluid jet amplifiers that served as passive AND units. This modification is shown in figure 6. Thus, when the passive AND unit was not delivering a signal, the control port and the interaction region vent of the output fluid jet amplifier would hopefully be at the same pressure. Even with this design change, the amplifier's performance sensitivity to interaction region vent V_1 pressure continued to be bothersome.

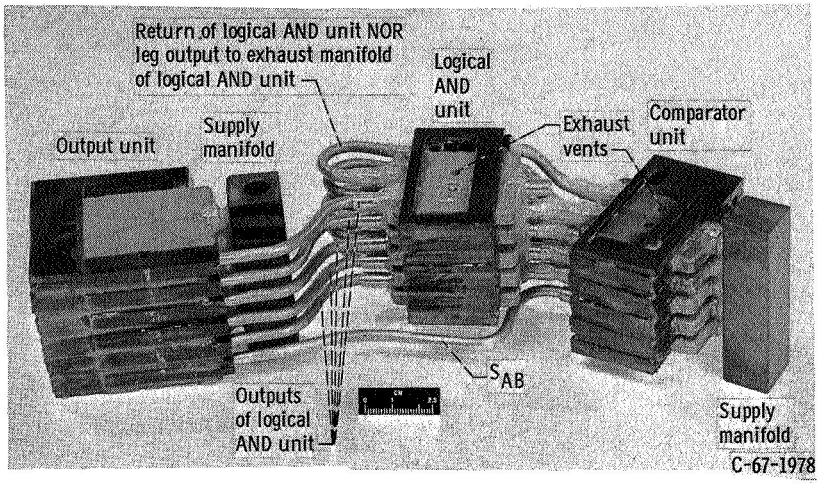

(a) Bottom view.

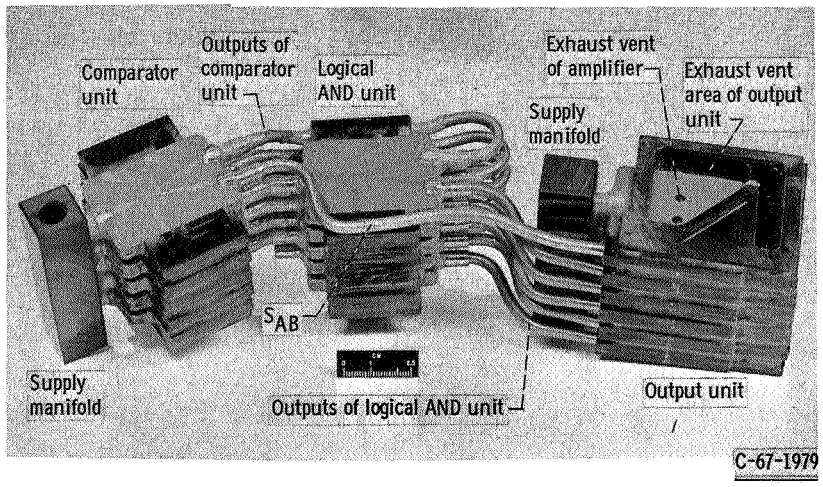

(b) Top view.

Figure 7. - Flueric shock position sensor without cover plates and exhaust manifolds.

Method of Fabrication

Standard commercially available Corning OR-NOR type fluid jet amplifiers of the type shown in figure 5 were used as the basic flueric components. An ambient atmosphere to the amplifiers' exhaust and control port vents as well as interconnections between elements was accomplished by cementing pieces of engraved phenolic board around the amplifiers. Three blocks of amplifiers cemented together with phenolic board

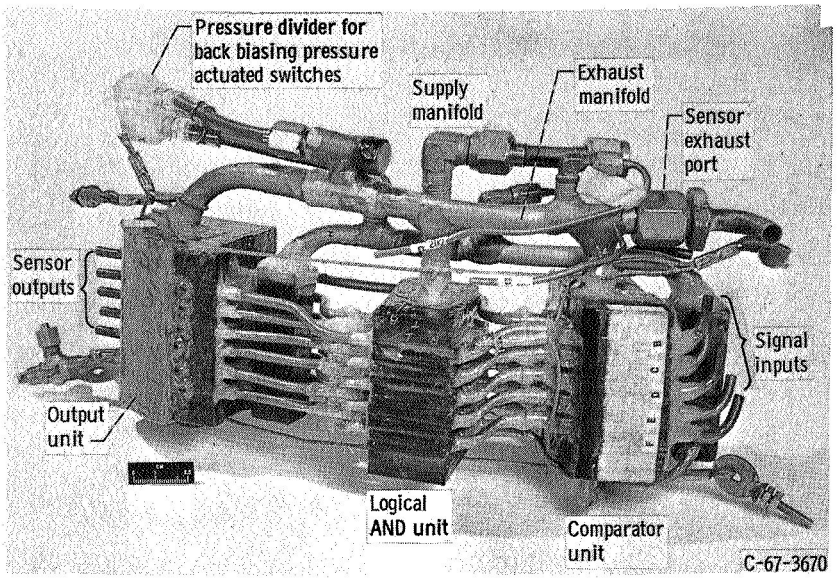

(a) Front view.

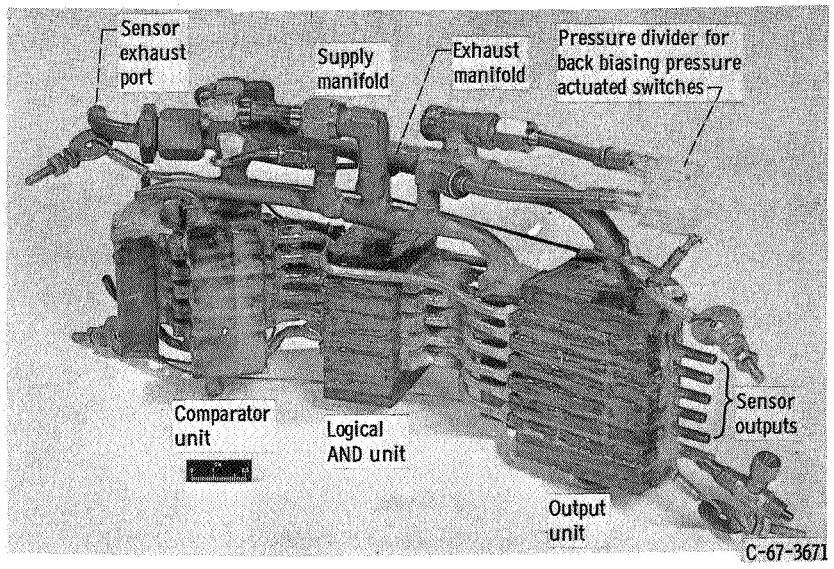

(b) Bottom view.

Figure 8. - Assembled shock position sensor.

were fabricated, corresponding to the three types of logic functions of figure 2. After the three functional blocks were fabricated and tested, they were interconnected with each other by means of properly sized copper tubing. Figures 7(a) and (b) show top and bottom views of the assembled shock position sensor minus the top and bottom cover plates and the associated supply and exhaust ducting. It is noted in the figures that the NOR leg outputs of the logical AND unit are returned to the AND unit exhaust instead of the control port vents of the output unit amplifiers. Routing the NOR leg outputs of the passive AND unit to the control port vents of the output unit was accomplished after these photographs were taken.

The complete sensor with cover plates and supply and exhaust ducting is shown in figure 8. To be noted is the size of the exhaust manifold. Its cross-sectional area is 9.4 times the sum of the power nozzle throat areas of the active fluid jet amplifiers in the sensor, and it represented the largest tube that could be packaged between the sensor and the available space in the inlet. As a result of the small exhaust tube area and the changing flows associated with amplifier switching, however, small waves and fluctuations are generated in the exhaust tube. Although the waves and fluctuations might be only a few percent of amplifier gage supply pressure, it is believed that they are still large enough to cause erratic operation of the AND and Output units (see appendix B).

EXPERIMENTAL RESULTS

Bench Tests

During fabrication of the prototype sensor, bench tests were performed on it during the various stages of assembly. The components worked reliably when used separately and when connected together as long as the exhaust manifold was absent. Installation of the exhaust manifold, however, gave rise to dynamic instabilities in the sensor's operation. The source of the instabilities appeared to be the presence of pressure gradients in the exhaust manifold which caused erratic triggering of the logical AND unit and possibly the output unit. The previously mentioned sensitivity of the OR-NOR type amplifiers (used as the AND units) to the interaction region vent V_1 pressures rendered the passive AND units particularly susceptible to small variations in the amplifier exhaust pressure (appendix B). A temporary solution to the problem, which rendered the sensor statically stable, was obtained by blocking the outputs of the output units. Dynamically, however, the sensor was marginally stable. As discussed in appendix B, future sensors should have much larger exhaust manifold cross-sectional areas to eliminate unwanted pressure waves. Reduction of the output stage supply to exhaust pressure ratio would have helped (appendix B), but, the ratio was left at the design value so that the units

could drive the available pressure actuated switches. The circuit of figure 6 was chosen over that of figure 3 at this time in an attempt to reduce some of the effects of exhaust manifold pressure waves.

A bench test of the sensor's static performance was conducted using the pressure distribution of figure 1. All pressures were multiplied by a constant factor of 2.9 so that they would be within the range of available laboratory instrumentation. As discussed in appendix A and noted in reference 7, such scaling of pressure levels is permissible as long as pressure ratios are not changed and the minimum operating Reynolds number of the fluid jet amplifiers is not approached. Results are given in table I. The symbols of table I correspond to those symbols on the curves of figure 1.

TABLE I. - BENCH TEST OF FLUERIC SHOCK POSITION SENSOR PRIOR TO WIND TUNNEL TESTING

[Pressure distribution of fig. 1 used for control signals; all pressures multiplied by a factor of 2.9; orifice hole distribution: taps A, B, E, and F, 0.070 in. (0.178 cm); tap C, 0.0465 in. (0.118 cm); tap D, 0.086 in. (0.203 cm).]

Curve symbol (fig. 1)	Sensor output				
	S''_{AB}	S''_{BC}	S''_{CD}	S''_{DE}	S''_{EF}
○	[a]X	X	X	X	X
□	O	X	X	X	X
▷	O	X	X	X	X
△	O	O	X	X	X
▽	O	O	O	X	X
◇	O	O	O	O	X
⬠	O	O	O	O	X

[a]On output, X; off output, O.

As can be seen by comparing table I and figure 1, the sensor gave a reasonably accurate indication of the shock wave position with the exception of the curves represented by the symbols ▷ and ⬠. Orifices were placed at the beginning of the sensor's input signal lines and, as noted in table I, the orifice sizes were not uniform. The purpose of the signal line orifices was (1) to provide single reflection termination to the

signal lines (0.125 in. (0.317-cm) inside diameter), (2) to reduce the maximum signals which would be delivered to the shock position sensor, and (3) to partially bias out some of the irregularities in the experimentally observed inlet wall pressure distribution. Biasing out of the wall pressure irregularities is responsible for the nonuniform sensor signal line orifice sizes. As will be shown shortly, the particular pressure tap orifice hole size distribution shown in table I may have been improper for optimum performance of the sensor under wind tunnel conditions.

Wind Tunnel Tests

Since the research inlet was being tested concurrently with the shock position sensor's bench tests, it was decided to mount the sensor in the inlet as a rider experiment to verify the laboratory results. The first set of static response tests in the wind tunnel was made when the aft boundary layer bleeds on the inlet were closed. The pressure dip at pressure tap D in figure 1 was thus eliminated. Figure 9 shows the sensor

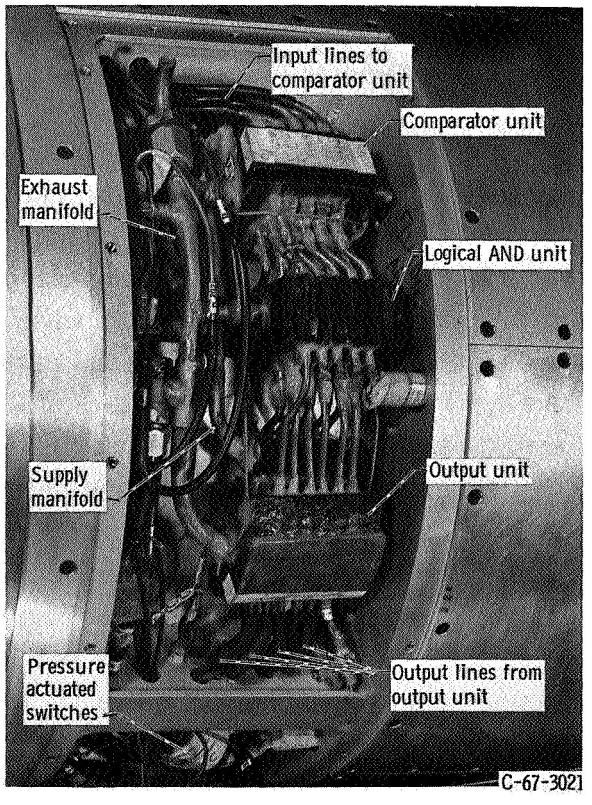

Figure 9. - Flueric shock position sensor installed in research inlet.

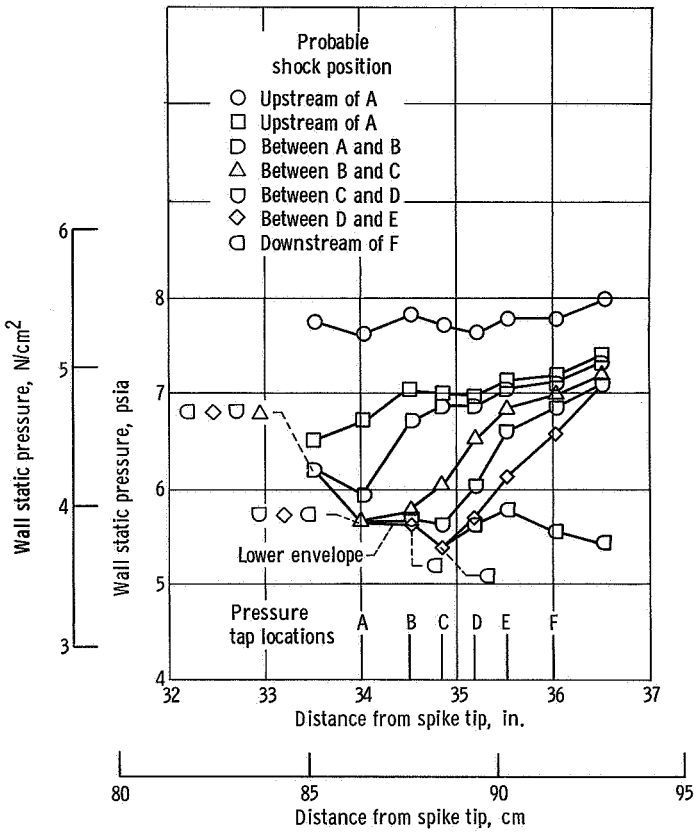

Figure 10. - Typical wall static pressure distributions as function of shock position. Aft boundary layer bleed closed.

installed in the inlet for these tests. Figure 10 shows the resultant wall pressure distribution as measured by a series of static pressure taps located at the same axial locations as the sensor's taps but displaced 60° around the circumference of the inlet.

Table II shows the static pattern of the sensor's outputs when the pressures of figure 10 were recorded. The symbols in table II correspond to those for the pressure distributions in figure 10. As can be seen, the output pattern of the shock position sensor gave a reasonably accurate indication of static shock position except for symbols ◇ and ▢. Subsequent to the wind tunnel tests used in obtaining the data of table II, the inlet was disassembled and the orifice holes at the beginning of the pressure tap lines were checked. It was found that a mistake had been made in installing the orifices. The measured hole diameters are given in table II and do not correspond with the hole distribution of table I. Nevertheless, the sensor performed well during the tests when the aft boundary layer bleeds were closed and, as will be shown later, it was possibly due to the inadvertent mixup of the orifice hole size distribution.

The aft boundary layer bleeds were reopened so that the wall static pressure distribution would be similar to that of figure 1. The actual pressure distribution obtained is

TABLE II. - STATIC OUTPUT OF FLUERIC SHOCK POSITION SENSOR

[Aft boundary layer bleed on inlet closed; orifice hole distribution: taps A, D, E, and F, 0.070 in. (0.178 cm); tap B, 0.086 in. (0.203 cm); tap C, 0.0465 in. (0.118 cm).]

Curve symbol (fig. 10)	Sensor output				
	S''_{AB}	S''_{BC}	S''_{CD}	S''_{DE}	S''_{EF}
○	[a]X	X	X	X	X
□	X	X	X	X	X
▷	O	X	X	X	X
△	O	O	X	X	X
▽	O	O	O	X	X
◇	O	O	O	O	X
◁	O	O	O	O	X

[a]On output, X; off output, O.

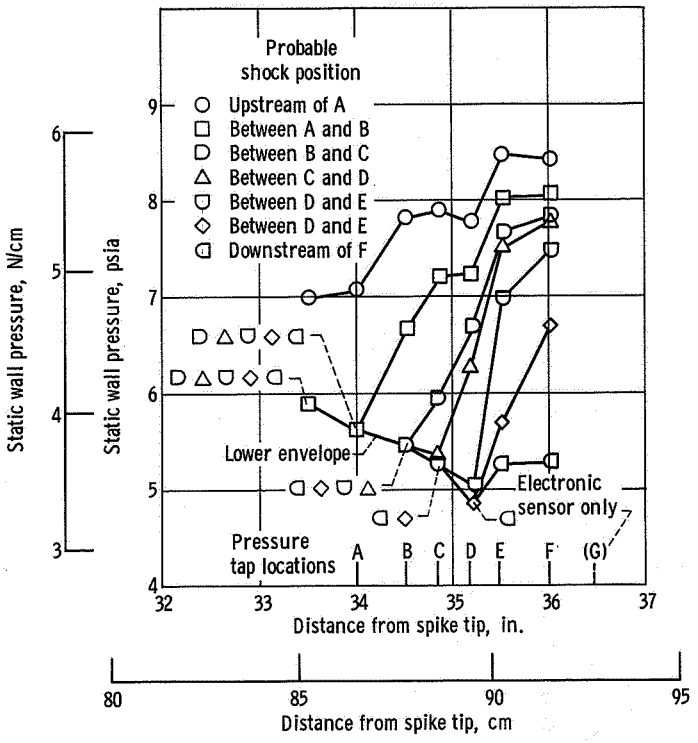

Figure 11. - Typical wall static pressure distributions as function of shock position. Aft boundary layer bleed reopened.

shown in figure 11. The flueric shock position sensor signal line orifices were resized to conform to the orifice hole size distribution given in table I.

An electronic shock position sensor was implemented and used as a check on the flueric sensor's output. The electronic sensor used output signals from static pressure transducers which measured the pressure distributions of figure 11. It should be remembered that the pressure taps for the flueric sensor and the pressure taps for the electronic sensor were at the same axial location but displaced 60° from each other around the circumference of the inlet. Pressure distributions in the inlet were assumed to be axisymmetric. Functionally, the electronic sensor was identical to the flueric sensor except that electronic biasing of the measured input signals was incorporated and the minimum in wall pressure closest to the throat (after bias values had been subtracted) was taken to be the true shock position. Output of the electronic sensor was checked against measured wall static pressure distributions and found, with the exception of location D, to give an accurate indication of normal shock position.

Table III shows simultaneous static output patterns of the flueric and electronic shock

TABLE III. - STATIC OUTPUTS OF FLUERIC AND ELECTRONIC SHOCK POSITION SENSORS

[Aft boundary layer bleed on inlet reopened; orifice hole distribution: taps A, B, E, and F, 0.070 in. (0.178 cm); tap C, 0.0465 in. (0.118 cm); tap D, 0.086 in. (0.203 cm).]

Electronic sensor output						Flueric sensor output				
S''_{AB}	S''_{BC}	S''_{CD}	S''_{DE}	S''_{EF}	S''_{FG}	S''_{AB}	S''_{BC}	S''_{CD}	S''_{DE}	S''_{EF}
[a]O	O	O	O	O	O	O	O	O	O	O
O	O	O	O	O	X	O	O	O	O	X
O	O	O	O	X	X	O	O	O	O	X
O	O	O	X	X	X	O	O	O	O	X
O	O	X	X	X	X	O	O	X	X	X
O	X	X	X	X	X	O	X	X	X	X
X	X	X	X	X	X	X	X	X	X	X
O	X	X	X	X	X	O	X	X	X	X
O	O	X	X	X	X	O	O	X	X	X
O	O	O	X	X	X	O	O	O	O	X
O	O	O	O	X	X	O	O	O	O	X
O	O	O	O	O	X	O	O	O	O	X
O	O	O	O	O	O	O	O	O	O	O

[a]On output, X; off output, O.

position sensors. Presence of a normal shock wave is indicated by a zero followed by an x. Because of foreign particle ingestion through the Pitot supply tube, the flueric sensor was not operating at the time the data of figure 11 were recorded. Thus, only the electronic sensor's outputs were available as a check on the flueric sensor's static performance.

As indicated by table III, the flueric sensor accurately tracked the electronic sensor for the three upstream shock positions - $\bar{S}''_{AB}$, S''_{AB}, and S''_{BC}. However, S''_{CD} and the absence of S''_{DE} could not be made to simultaneously occur on the flueric sensor's outputs. Instead, the flueric sensor behaved as if the shock were unstable at position CD and flipped rapidly back and forth between BC and DE. The apparent shock location tended to prefer station DE and did not progress to station EF as rapidly as it should have (i.e., S''_{EF} did not become zero on the flueric sensor's output as soon as it did on the electronic sensor's output). If the sensor was not malfunctioning because of ingested foreign particles (see Foreign Particle Ingestion section), the output pattern observed in table III was typical and repeated both during a run and from run to run. Lights were connected to both the output switches of the flueric sensor and also the outputs of the electronic sensor, so that the progress of indicated shock position could be observed visually. The output of the flueric sensor was observed to be unstable and to oscillate rapidly when the electronic sensor registered a shock location between taps C and D (output S''_{CD}).

The preceding performance anomaly contrasted with the fact that the flueric sensor worked well, statically, when the boundary layer bleeds aft of the shock were closed. The following are possible explanations for this decreased static performance:

(1) When the boundary layer bleeds were open, the pressures at C and D were observed to be very noisy when the shock was either on or between these two taps.

(2) The dynamic performance of the sensor tended to be erratic, especially for shock positions in the range of taps C and D (see Dynamic Tests).

(3) It is theorized that these noisy signals, resulting from boundary layer bleed-shock wave interactions, excited the flueric shock sensor and drove it into unstable oscillations.

Thus, it is possible that, although the sensor's static response was being evaluated, its dynamic response kept it from functioning properly. This explanation could also account for the fact that identical pressure distributions applied under laboratory conditions resulted in correct sensor output patterns. The laboratory pressures were highly noise free and, hence, did not excite the sensor into spurious oscillations.

Another possible explanation for the decreased static performance of the sensor is that its performance characteristics changed during the course of the wind tunnel testing. To check this hypothesis, the sensor was again bench tested after completion of the wind tunnel runs. Tables IV and V show static response of the sensor using scaled pressure distributions of figures 1 and 11 and using the signal line orifice hole distribution of

TABLE IV. - BENCH TEST OF FLUERIC SHOCK POSITION SENSOR FOLLOWING WIND TUNNEL TESTING

[Pressure distribution of fig. 1 used for control signals; all pressures multiplied by a constant factor of 2.72; orifice hole distribution, taps A, B, E, and F, 0.070 in. (0.178 cm); tap C, 0.0465 in. (0.118 cm); tap D, 0.086 in. (0.203 cm).]

Curve symbol (fig. 1)	Sensor output				
	S''_{AB}	S''_{BC}	S''_{CD}	S''_{DE}	S''_{EF}
○	[a]O	O	O	X	X
□	O	O	O	X	X
▷	O	O	X	X	X
△	O	O	O	X	X
▽	O	O	O	X	X
◇	O	O	O	O	X
◁	O	O	O	O	X

[a]On output, X; off output, O.

TABLE V. - BENCH TEST OF FLUERIC SHOCK POSITION SENSOR FOLLOWING WIND TUNNEL TESTING

[Pressure distribtuion of fig. 11 used for control signals; all pressures multiplied by a constant factor of 2.9; orifice hole distribution: taps A, B, E, and F, 0.070 in. (0.178 cm); tap C, 0.0465 in. (0.118 cm); tap D, 0.086 in. (0.203 cm).]

Curve symbol (fig. 11)	Sensor output				
	S''_{AB}	S''_{BC}	S''_{CD}	S''_{DE}	S''_{EF}
○	[a]X	X	X	X	X
□	O	[b]O	[b]O	X	X
▷	O	O	X	X	X
△	O	O	O	X	X
▽	O	O	O	O	X
◇	O	O	O	O	X
◁	O	O	O	O	X

[a]On output, X; off output, O.

[b]Raising the signal pressure to tap C or B causes sensor outputs S''_{BC} and S''_{CD} to give an "on" output (X) for curve symbol □.

table I. As can be seen from tables IV and V, the sensor, in the post wind tunnel bench tests, did not give a good static representation of the effective normal shock position. The reasons for its inability to reproduce its performance prior to wind tunnel testing are not known, but it is suspected that foreign particle ingestion or a gradual buildup of contaminants in the flow passages of the sensor's component fluid jet amplifiers is responsible.

As suggested by tables IV and V, the result of this performance change effectively rendered the signal line C restricting orifice too small. A slight increase in the pressure applied to tap C yielded correct sensor output patterns. (In other words, raising the signal pressure to tap C by 14 percent makes table IV identical with table I except S''_{AB} is "on" in the second row (curve symbol □).) Thus, the experimentally determined orifice hole distribution listed in table I may have become incorrect during the sensor's operation in the wind tunnel.

A new set of orifice hole sizes for the input signal lines was determined and the sensor again bench tested with the static wall pressure distributions of figures 1 and 11. Its performance is shown for these two cases, respectively, in tables VI and VII. The orifice hole distributions are listed in the tables. As can be seen by comparing the tables with their respective figures, the second bench test of the sensor yielded outputs which

TABLE VI. - BENCH TEST OF FLUERIC SHOCK POSITION SENSOR WITH IMPROVED ORIFICE HOLE DISTRIBUTION

[Pressure distribution of fig. 1 used for control signals; all pressures multiplied by a constant factor of 2.72, orifice hole distribution: taps A, B, C, D, and F 0.070 in. (0.178 cm); tap E, 0.0465 in. (0.118 cm).]

Curve symbol (fig. 1)	Sensor output				
	S''_{AB}	S''_{BC}	S''_{CD}	S''_{DE}	S''_{EF}
○	[a]X	X	X	X	X
□	O	X	X	X	X
▷	O	O	X	X	X
△	O	O	O	X	X
▽	O	O	O	O	X
◇	O	O	O	O	X
⬠	X	X	X	X	X

[a]On output, X; off output, O.

TABLE VII. - BENCH TEST OF FLUERIC SHOCK POSITION SENSOR WITH IMPROVED ORIFICE HOLE DISTRIBUTION

[Pressure distribution of fig. 11 used for control signals; all pressures multiplied by a constant factor of 2.9; orifice hole distribution: taps A, B, C, D, and F, 0.070 in. (0.178 cm); tap E, 0.0465 in. (0.118 cm).]

Curve symbol (fig. 11)	Sensor output				
	S''_{AB}	S''_{BC}	S''_{CD}	S''_{DE}	S''_{EF}
○	[a]X	X	X	X	X
□	O	X	X	X	X
⌐	O	O	X	X	X
△	O	O	O	X	X
⌐	O	O	O	O	X
◇	O	O	O	O	X
⌐	X	X	X	X	X

[a]On output, X; off output, O.

accurately indicated effective shock wave positions with the single exception of the most rearward shock wave position.

In summary, the decreased static performance of the shock position sensor could have been caused by either of the two previously mentioned effects. In all likelihood, it was a combination of both - the improper orifice hole distribution rendering the shock position sensor less stable and leaving less margin of error between the pressures which were presented to the sensor, and those for which the sensor would not operate. This decreased stability and the reduction of the range of acceptable signal pressures rendered the sensor more susceptible to the high frequency noise which was present on taps C and D when the shock wave was in the vicinity of the boundary layer bleeds.

Dynamic Response of the Sensor

Dynamic response tests were conducted on the bench at each stage of sensor assembly. After assembly, both bench and wind tunnel dynamic tests were performed. The bench tests on the sensor's component amplifiers and functional blocks before interconnection indicated approximately 0.0005-second switching times. Prior to installation

of the exhaust manifolds, the complete shock sensor exhibited response times of approximately 0.0005 second per amplifier plus the time required for propagation of the signals along interconnection lines. Presence of the exhaust manifold, however, made response of the sensor erratic and, at times, unstable. As mentioned previously, the sensor was stabilized by connecting switches to its output. These switches constituted blocked loads. Capacitance and diaphram movement were negligible. After suitable adjustments, the flueric sensor, under laboratory conditions, exhibited flat response at both full and half amplitude for cyclic input frequencies up to 115 hertz. It should be noted that, in the laboratory, it was not possible to cyclicly apply the pressure distributions of figures 10 or 11. Instead, all signal inputs were held at sensor exhaust pressure except for one which was changed in a cyclic, stepwise manner with a slotted disk valve.

Following bench dynamic tests, the flueric shock sensor's dynamic response was evaluated in the wind tunnel. The dynamic tests were conducted in two phases: (1) passing the inlet's throat shock back and forth over all of the flueric sensor's taps, and (2) passing the throat shock back and forth over only a fixed number of the sensor's taps. Since the dynamic response of the inlet shock position was not a frequency insensitive function of the inlet bypass door opening, which was used to disturb shock position, the latter sensor dynamic test was more difficult to conduct.

The full-amplitude wind tunnel shock sensor response tests are shown in figures 12 and 13(a) to (g). It is seen that full-amplitude response can be obtained from the flueric sensor for shock cyclic disturbance frequencies in excess of 60 hertz. Reduced-amplitude tests are shown in figures 14 and 15. Test conditions for figure 14 were identical to those for figure 13. Figures 15(a) to (d) show indicated flueric sensor output in parallel with pressure transducer recordings of the electronic sensor's inputs. When the

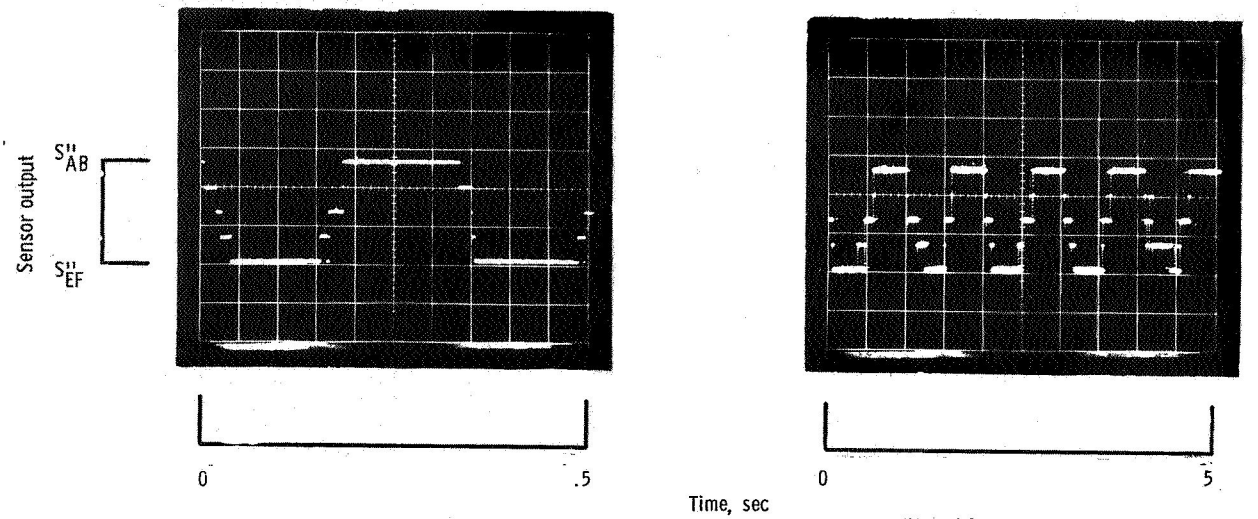

(a) Test frequency, 3.0 cps. (b) Test frequency, 9.7 cps.

Figure 12. - Dynamic response of flueric shock sensor. Aft boundary layer bleeds closed.

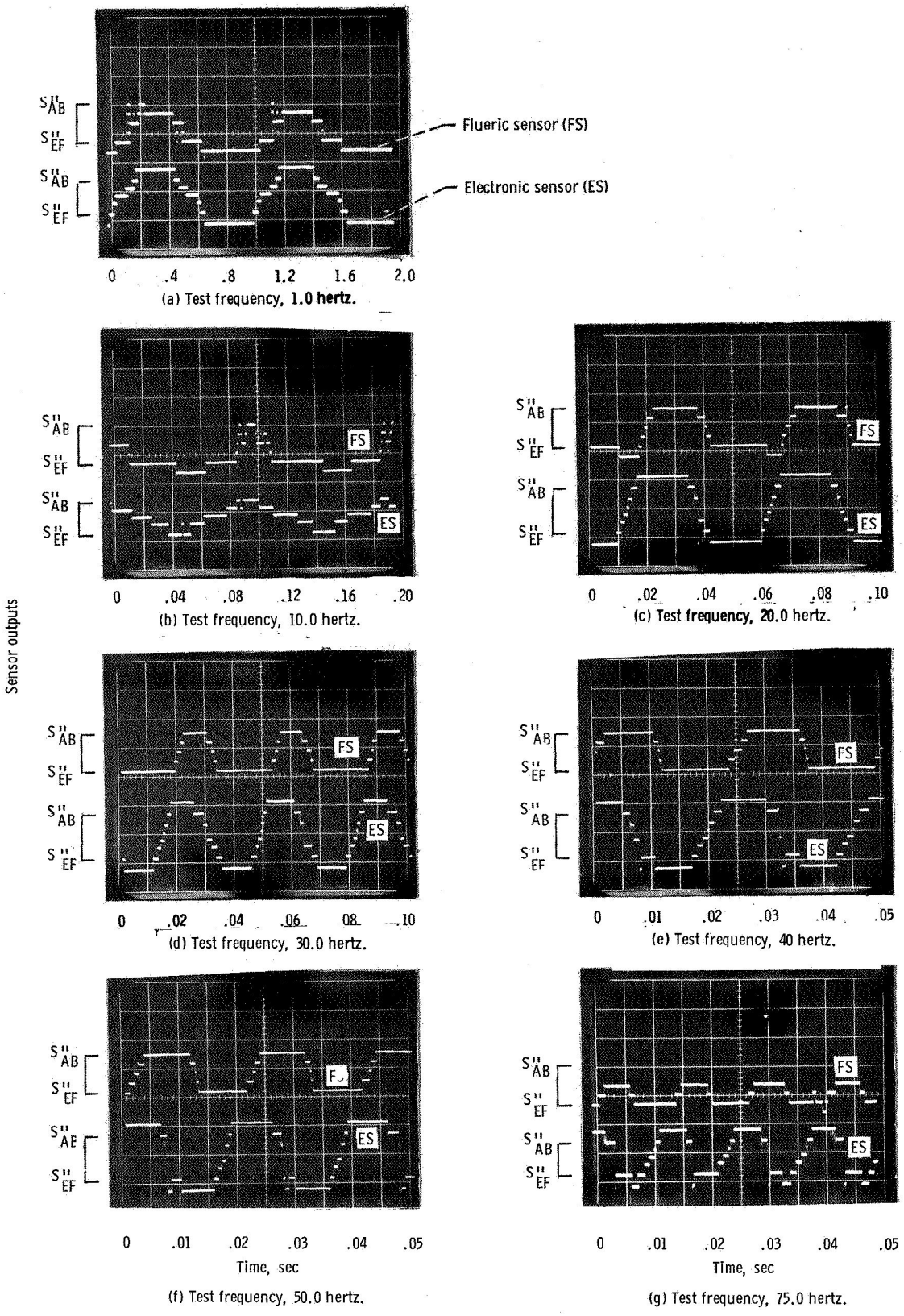

Figure 13. - Dynamic response of flueric and electronic shock position sensors. Aft boundary layer bleeds reopened.

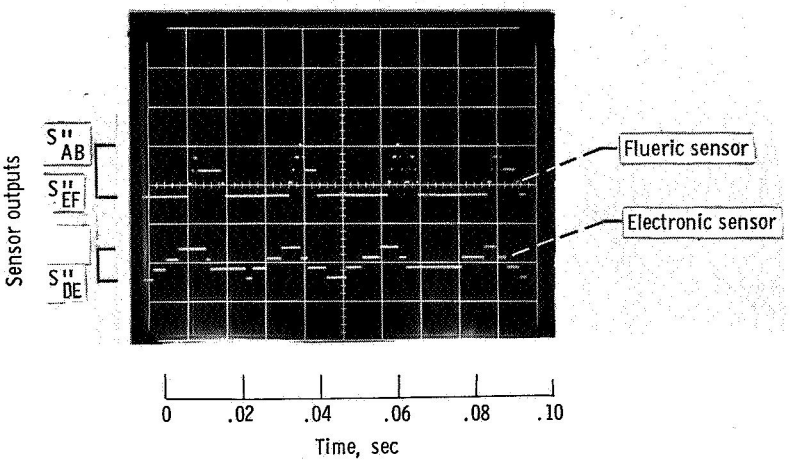

Figure 14. - Dynamic response of flueric and electronic shock position sensors at reduced shock excursions. Aft boundary layer bleeds reopened.

shock crosses a pressure tap, the trace rises from its low-noise supersonic flow value to a high-noise subsonic flow value. The supersonic flow values for the various pressure taps are given the value (0 N/cm^2) in figure 15.

Figures 14 and 15 indicate that the apparently high dynamic response suggested by data from figure 13 might be more apparent than real. Figure 15(a) shows that the flueric sensor does not track measured shock amplitude accurately for test frequencies as low as 13.5 hertz. At higher frequencies, such as 20.7 hertz in figure 15(b) or 60.1 hertz in figure 15(d), the sensor output usually indicates two shock positions with an occasional jump to three or four shock positions. However, as seen from figure 15(b), where only two output shock positions are indicated by the flueric sensor, actual shock excursion ranges from S''_{FG} to S''_{BC}. The flueric sensor, for the case of figure 15(b) should have been indicating at least four shock positions. The erratic dynamic performance shown in figures 14 and 15 suggests that the same instabilities and performance degradations noted in the laboratory when the sensor's exhaust manifolds were installed are present and causing the flueric sensor to malfunction in the wind tunnel.

Foreign Particle Ingestion

A substantial amount of difficulty was experienced with foreign particle ingestion. The presence of foreign particles in the flueric sensor was manifested by erratic performance of the sensor's outputs. Output patterns would occur which were incompatible with the interconnection between output amplifiers. During a run, such patterns would exist for a period of time and then change to a normal arrangement as the sensor apparently cleared itself.

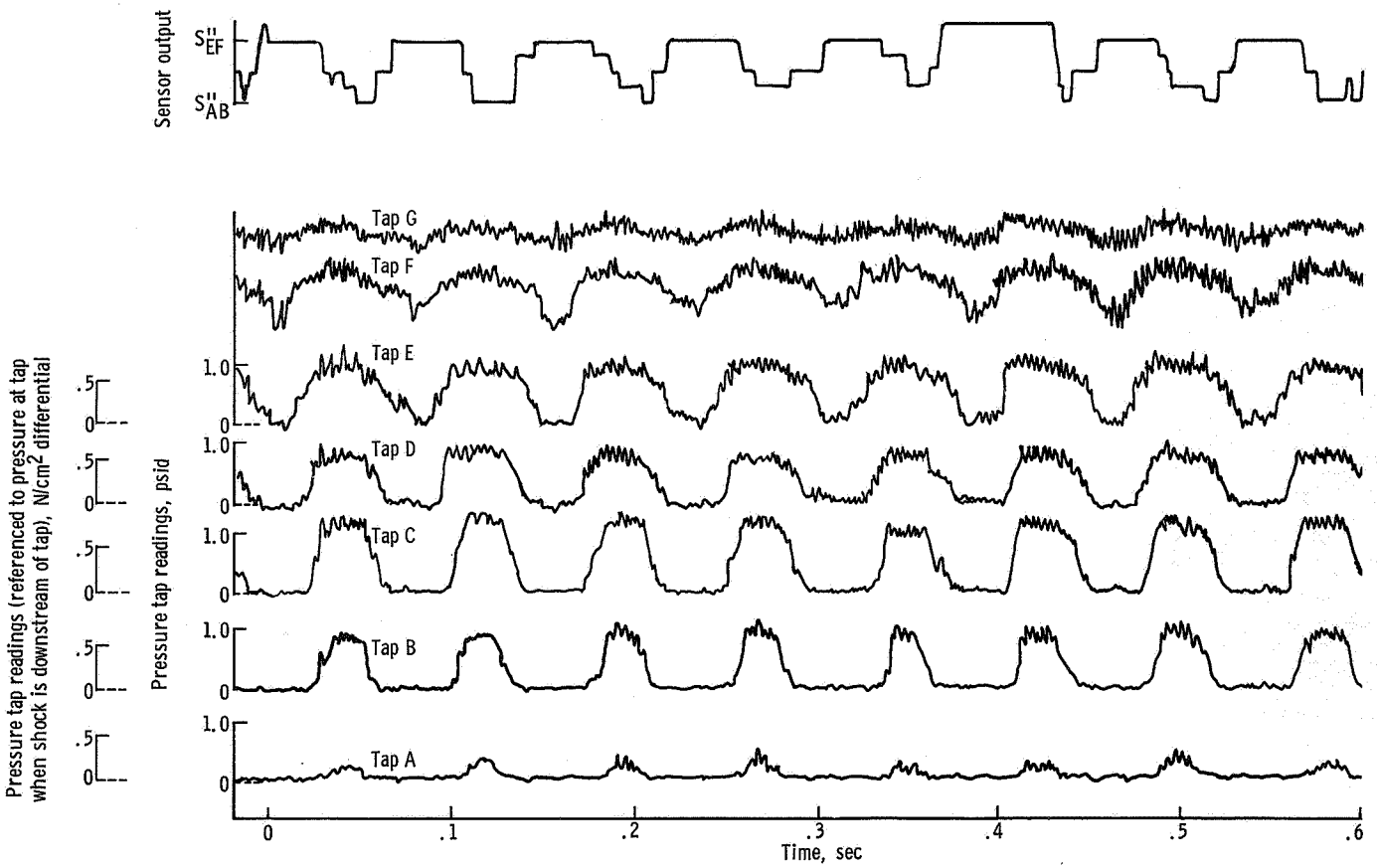

(a) Test frequency, 13.5 hertz.

Figure 15. - Pressure tap readings and sensor output. Aft boundary layer bleed closed.

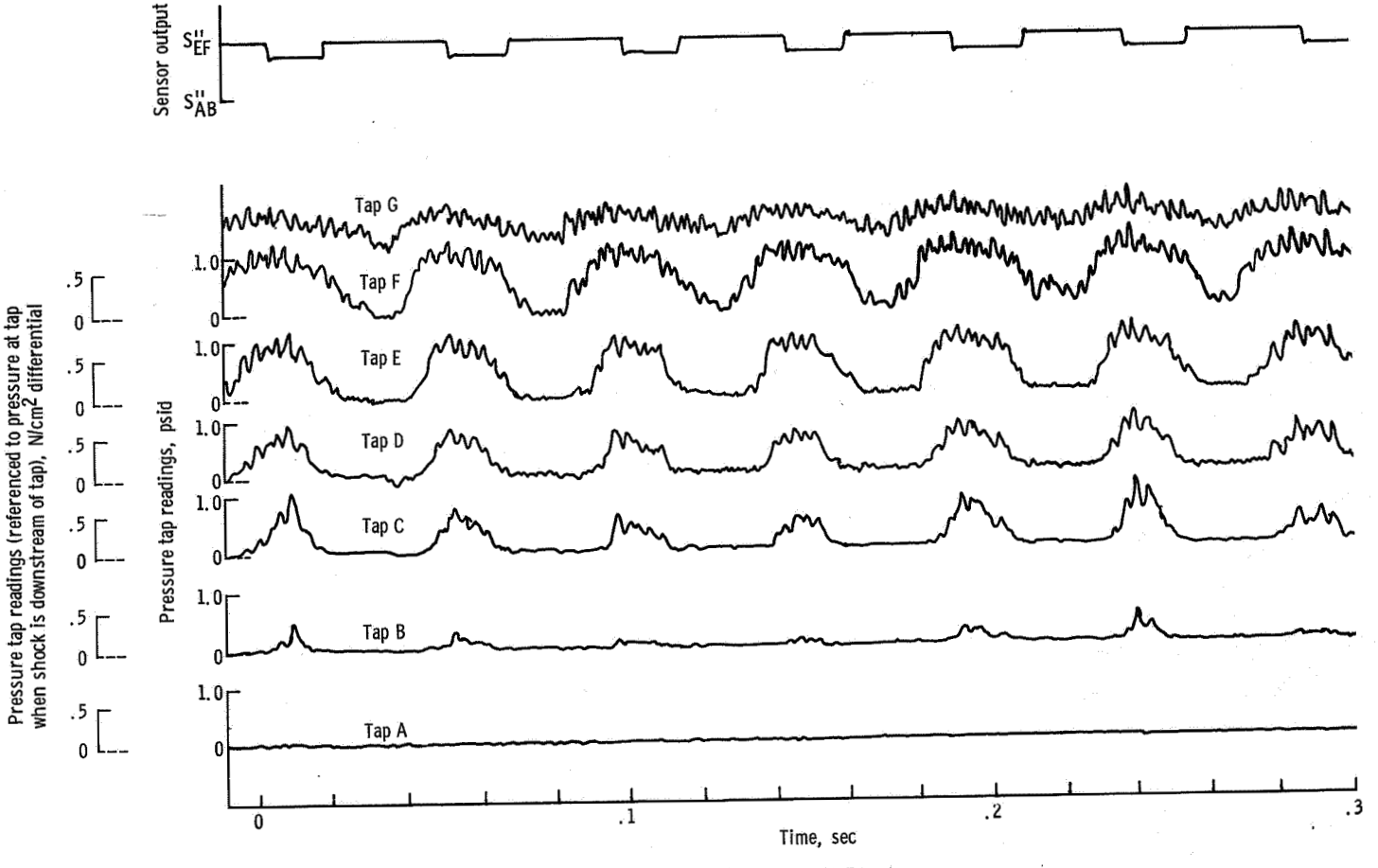

(b) Test frequency, 20.7 hertz.

Figure 15. - Continued.

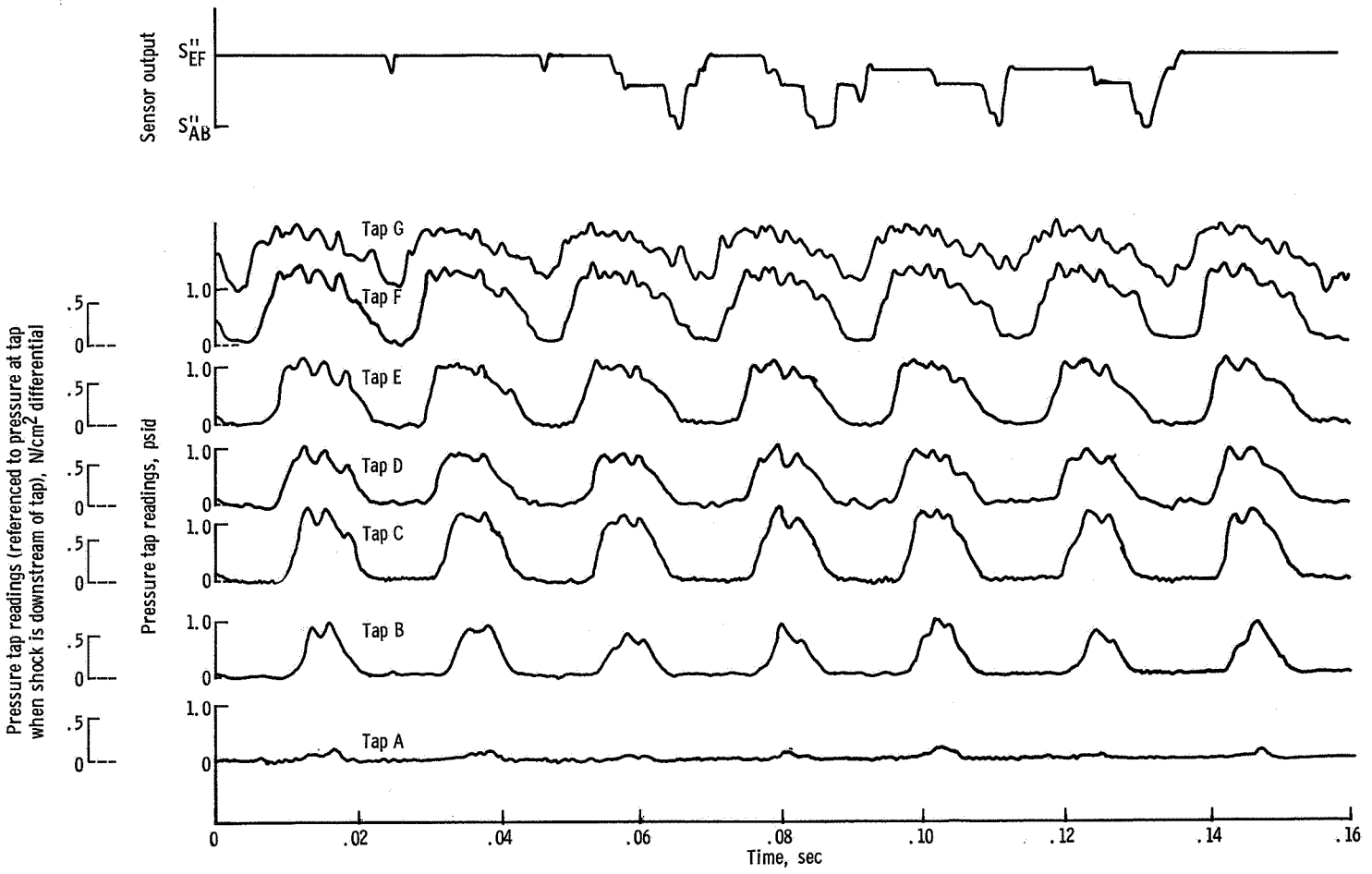

(c) Test frequency, 45.5 hertz.

Figure 15. - Continued.

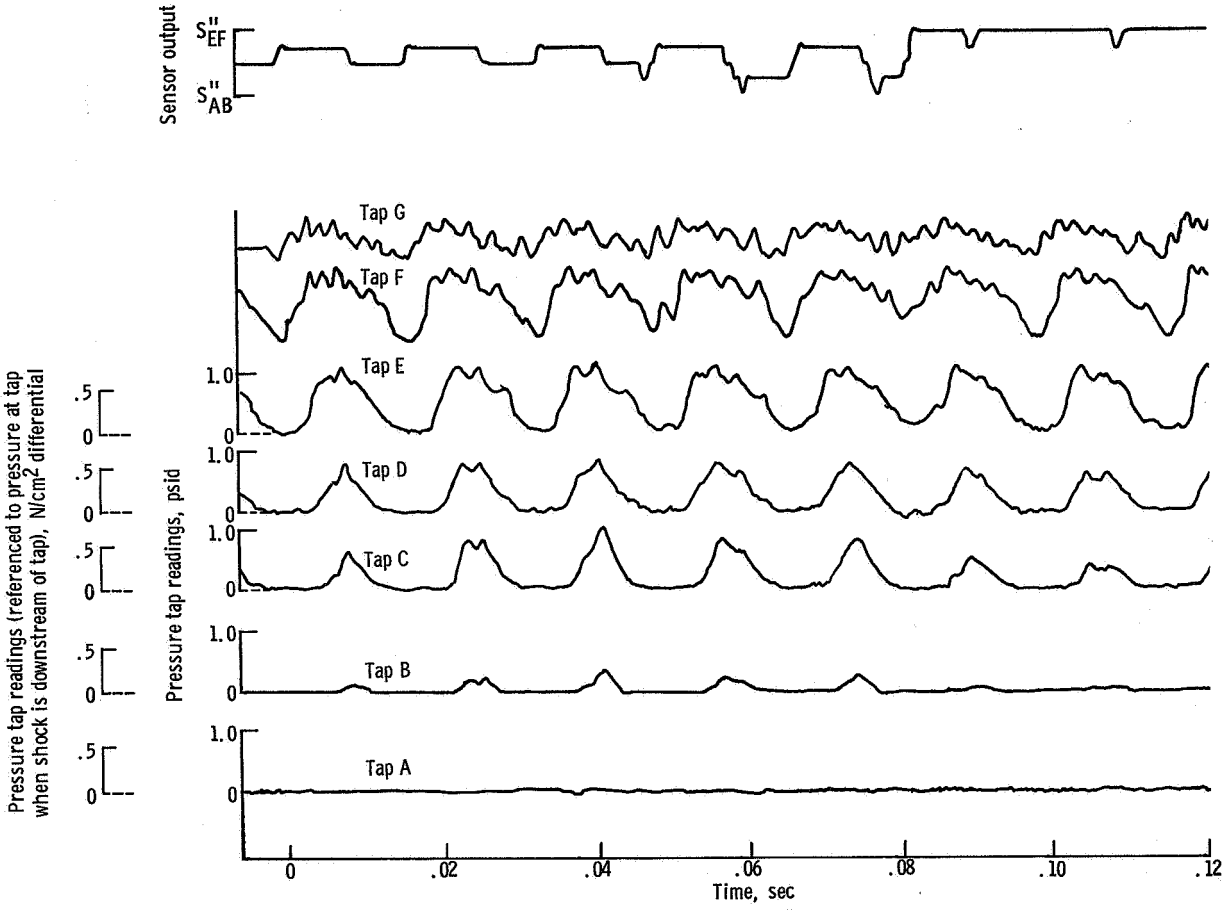

(d) Test Frequency, 60.1 hertz.

Figure 15. - Concluded.

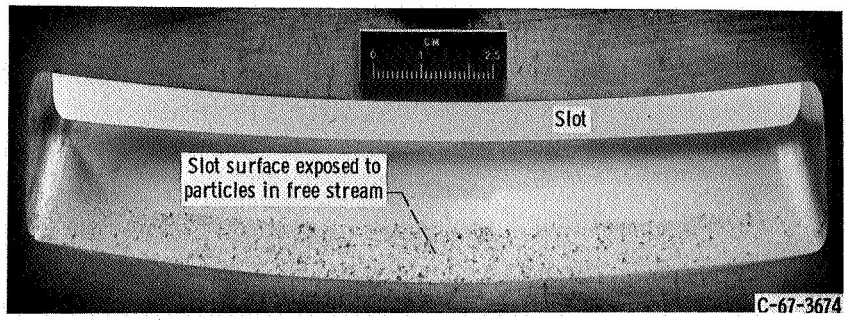

Figure 16. - Exposed inlet surfaces showing pitting from particles in free stream.

The source of the foreign particles is believed to be small pieces of alumina from the dryer beds of the wind tunnel. These pieces of alumina were carried along by the main flow of the tunnel, accelerated through the test section, and impacted on the research inlet. The flow which entered the inlet carried the particles, and a portion of them were swallowed by the forward facing Pitot tube which supplied the flueric shock position sensor. Figure 16 shows a portion of the inlet's slotted external surface. The downstream surfaces of the slots were inclined at an angle of approximately 45^{o} to the free stream flow. That portion of the downstream slot surface which is not shaded from the approaching particles shows marked pitting. On the basis of impact counts made on this pitted surface, it was estimated that between 50 and 100 particles might have entered the sensor's supply tube and passed through the sensor's internal passageways. Since the power nozzles of the amplifiers used in the sensors were only 0.020 inch (0.0508 cm) wide and the craters left by the impacting particles were as large as 0.030 inch (0.0763 cm) in diameter, ample opportunity existed for the clogging of the amplifiers' passageways. Clearly, a requirement for future sensors, whether used in wind tunnels or in operational flight inlets, is the use of a particle trap and filter in the supply manifold. In addition, flow sources, located at the junction of the signal lines with the sensor inputs, should be used to reverse flow the signal lines with clean air. Thus, the signal lines would discharge air into the inlet instead of taking air and dirt particles from it. Since the reverse signal line flow would be constant and low (thus incurring low frictional pressure drops), pressure fluctuations at the wall static pressure taps would be transmitted accurately to the inputs of the shock position sensor.

DISCUSSION OF RESULTS

Performance of Sensor

For the inlet configuration which had no aft boundary layer bleeds, the flueric sensor exhibited satisfactory static performance. When the aft boundary layer bleeds were

opened and the distribution of the sensor's signal line orifices was changed, the sensor's static output became oscillatory and inaccurate when the shock wave was in the vicinity of the boundary layer bleeds (between pressure taps C and D). This degradation in static performance is believed to be caused by (1) marginal dynamic stability of the sensor which causes it to be highly sensitive to the noise in the input signals which occurs when the shock is in the vicinity of the boundary layer bleeds, and (2) a change in the sensor's operating characteristics that occurred during the course of the wind tunnel testing. The marginal dynamic sensitivity is believed to be caused by pressure waves in the exhaust manifold. A larger cross-sectional flow area manifold is clearly indicated. The change in sensor operating characteristics during wind tunnel testing is believed to be a result of foreign particle ingestion. Filtration of the supply flow and reverse flowing the signal lines should eliminate this latter problem.

Dynamic response of the sensor is not established. Laboratory bench tests were conducted at 115-hertz cyclic frequencies for various shock excursion amplitudes. The sensor could be adjusted to perform properly in these tests. However, when the actual static wall pressures of the inlet were applied to the sensor during wind tunnel tests, dynamic performance of the sensor was much lower than 115 hertz. Full-amplitude response of the sensor could be obtained for shock cyclic frequencies in excess of 50 hertz, but less than full-amplitude response could not be obtained at test frequencies as low as 13.5 hertz. The dynamic interactions in the exhaust passages of the sensor are believed to be responsible for its degraded dynamic response in the wind tunnel tests. A major contributing cause of the sensor's dynamic sensitivity to exhaust pressure fluctuations is probably the extreme switching sensitivity of the fluid jet amplifier OR-NOR units to vent V_1 pressures. This subject is treated in greater detail in appendix B.

As a result of the bench and wind tunnel tests of the flueric shock position sensor, a number of improvements can be suggested to upgrade its performance:

(1) The gage supply pressure to the output stage should be lowered by a factor of two. The ability of the logical AND unit to drive the output stage is marginal. If the supply to exhaust pressure drop of the output stage were reduced by a factor of two, the driving capability of the logical AND unit would be more than adequate.

(2) Future flueric shock position sensors should be fabricated using integrated flueric circuit techniques. This would enable a large reduction in overall sensor volume and lengths of internal sensor passageways. Size would be reduced and speed of response increased. Additionally, more space would be available for large cross-sectional area exhaust passageways.

(3) In conjunction with fabrication of the sensor using flueric integrated circuit techniques, the height of the power nozzles of the fluid jet amplifiers used in the circuit should be reduced by a factor of two. Flow consumption of the circuit would be reduced by a factor of two. Thus, for the same total circuit flow consumption, twice as many

samples of wall pressure and twice as many indicated output shock positions could be obtained. Conversely, for the same, fixed cross-sectional flow areas in the exhaust manifold, the exhaust manifold area to power nozzle area ratio would be doubled, thus decreasing the effect of pressure drops and waves in the exhaust manifold.

(4) Filtration of the supply and reverse flowing the signal lines is mandatory.

CONCLUSIONS

It is concluded that a flueric shock position sensor is feasible. The sensor described in this report accurately measured normal shock position when the inlet's aft bleeds were plugged. When the aft boundary layer bleeds were unplugged, the sensor gave reasonably accurate indications of shock position when the shock was not in the vicinity of the boundary layer bleeds. The sensor's static performance should be markedly improved by relatively simple changes to the existing circuit.

Dynamic response of the sensor was well behaved with the exhaust manifold removed, but erratic with the exhaust manifold installed. In the wind tunnel, better behavior was observed for large shock position excursions than with small excursions. It is believed that these effects were caused by inadequate exhaust passageway sizes. Appropriate changes to the sensor's exhaust manifold size and supply pressures should enable the sensor's dynamic performance to be improved markedly. A goal should be partial or full-amplitude response in excess of a 50 hertz minimum.

Erratic response and malfunctioning of the sensor was caused by foreign particles ingested through its supply tube. The particles would clog the small passageways of the fluid jet amplifiers. This problem should be even more severe for an operational sensor mounted in an aircraft's inlet. Filtration of the supply flow and reverse flowing of the signal lines will be necessary to eliminate foreign particle ingestion.

It is also concluded that significant decreases in sensor size and flow consumption are possible by the use of flueric integrated circuit techniques.

Lewis Research Center,
National Aeronautics and Space Administration,
Cleveland, Ohio, August 8, 1968,
126-15-02-20-22.

APPENDIX A

SCALING AMPLIFIER SIZES AS A FUNCTION OF OPERATING PRESSURE AND TEMPERATURE

For a digital, wall attachment fluid jet amplifier of given geometry, two operational restrictions determine a minimum size which can be used for a given supply gas total pressure and temperature. These restrictions are the following:

(1) The maximum power nozzle throat Mach number M_{max} at which the amplifier will still satisfactorily operate

(2) The minimum throat Reynolds number Re_{min} at which the fluid jet amplifier will satisfactorily operate

As pointed out in reference 4, and also as verified experimentally during this development program by Lewis Research Center, the performance of an amplifier may be considered to be relatively Reynold's number insensitive and pressure ratio insensitive as long as it is not operating in the vicinity of these limits.

Given the two limits of M_{max} and Re_{min}, it is possible to determine the minimum exhaust pressure at which a fluid jet amplifier of given geometry and size may operate. The power nozzle throat Reynolds number may be written

$$Re = \frac{\rho V_j D_j}{\mu g_o} = \frac{k p_j V_j D_j}{(k g_o R T_e)\mu} = \frac{k M_j p_j D_j}{\mu c_j} \tag{A1}$$

Regrouping and substituting the simultaneous limits of M_{max} and Re_{min} into equation (A1) gives

$$(p_j)_{min} = \left(\frac{c_j \mu}{k D_j}\right)\left(\frac{Re_{min}}{M_{max}}\right) \tag{A2}$$

The first term in equation (A2) is an effective shearing stress and depends only on the speed of sound in the gas c_j at the power nozzle exit, the viscosity μ of the gas, and the amplifier's power nozzle throat width D_j. Thus, for a supply gas of given composition and temperature and for a given amplifier size, the first term in equation (A2) is fixed.

The second term in equation (A2) is composed of the minimum Reynolds number and the maximum throat Mach number terms. These terms are a function of the amplifier geometry alone and do not depend on the properties of the supply gas. Thus, it is

seen that the right-hand side of equation (A2) contains two groups, one which is solely a function of the supply gas properties and amplifier size, and the other which is solely a function of the amplifier geometry.

As pointed out in the text, the exhaust pressure p_e for the fluid jet amplifiers in the shock position sensor should be approximately equal to the inlet's wall static pressures upstream of the shock wave. Since the power nozzle exit pressure p_j is approximately equal to exhaust pressure,

$$p_j \approx p_e \approx p_{th} = \left(\frac{p_{th}}{p_o}\right) p_o \tag{A3}$$

Equation (A3) may be substituted into equation (A2) to determine the minimum free stream total pressure p_o at which the shock position sensor may operate and still have an internal exhaust pressure p_e equal to the supersonic throat static pressure of the inlet. For this condition, p_o would equal p_s. Thus,

$$p_o = p_{s,min} = \frac{c_j \mu}{kD_J} \frac{Re_{min}}{M_{max}} \frac{1}{p_{th}/p_o} \tag{A4}$$

It was assumed that the amplifier used for fabricating the shock position sensor had a maximum power nozzle Mach number limit of 0.9, a minimum power nozzle Reynolds number of approximately 2340, and a power nozzle throat width D_j of 0.020 inch (0.0508 cm). Conditions of the air in the inlet throat were

$$p_s = 13.15 \text{ psia } (0.07 \text{ N/cm}^2)$$

$$T_o = 547^\circ \text{ R } (318 \text{ K})$$

$$p_{th}/p_o = 0.386$$

These conditions give the following properties at the fluid jet amplifier's throat:

$$T_3 = (T_J/T_o)\, T_o = (0.861)(574) = 493^\circ \text{ R } (275 \text{ K})$$

$$\mu_j = 2.5\times10^{-9} \text{ (lb force)(sec)/in.}^2 \text{ } (1.72 \text{ (N)(sec)/cm}^2)$$

$$c_j = 1.31\times10^4 \text{ in./sec } (3.33\times10^4 \text{ cm/sec})$$

Substituting the previous values into equation (A4) gives

$$p_{s,min} = \frac{(1.17\times10^{-3})(2600)}{(0.386)} = 7.88 \text{ psia } (5.43 \text{ N/cm}^2)$$

which is satisfactorily less than the 13.15 psia (9.07 N/cm^2) actually delivered to the amplifier. For the inlet's design free stream Mach number of 2.5, $p_{o,min}$ would correspond to a pressure altitude of 0.461 psia (0.318 N/cm^2) or approximately 77 600 feet (25 200 m). The next smaller, geometrically similar amplifier had a power nozzle width of 0.010 inch (0.0254 cm). This would have given a minimum free stream total pressure of 15.8 psia (10.9 N/cm^2). Since the wind tunnel was to be run at 13.1 psia (9.02 N/cm^2) total pressure, the smaller amplifier could not be used.

It should be noted that, under actual flight conditions of Mach 2.7 at 70 000 feet (21 400 m)(typical values for a supersonic transport), free stream total temperature would rise to 968° R (537 K). This higher total temperature would increase both the speed of sound and the viscosity of the supply gas to the sensor, thus decreasing the pressure altitude at which the sensor could satisfactorily operate. The minimum free stream total pressure under these latter conditions would be p_o = 15.1 psia (10.4 N/cm^2). At Mach 2.7, this would correspond to a pressure altitude of 0.648 psia (0.448 N/cm^2) or approximately 70 000 feet (21 400 m).

APPENDIX B

INTERCONNECTION OF THE CIRCUIT ELEMENTS

This appendix deals with the procedures used to interconnect the sensor's flueric elements and a brief analysis of some of the interconnection problems encountered. The details of digital flueric element interconnection are not covered here since they are dealt with adequately in other literature. Reference 5 provides a good general background. Reference 3 gives a detailed treatment of single reflection line termination which was used extensively in the sensor.

Interconnection of the sensor's inputs with the inlet's static wall pressure taps necessitated rather long lines - of the order of 18 to 20 inches (46 to 51 cm). Because of the length of the lines, some means of acoustically dampening reflected waves in the lines was necessary if high-speed response of the sensor was to be obtained. Acoustical termination yielded lines of such small diameter that high frictional pressure drops resulted. While the sensor could be adjusted to operate with these pressure drops at any one given set of flight conditions, a change in altitude, free stream total pressure, or temperature would possibly change the frictional pressure drops sufficiently to yield the sensor inoperative. Single reflection of the signal lines by means of an orifice at the beginning of the line was chosen instead. The orifice restriction was accomplished by drilling a hole in the inlet wall which was smaller in diameter than the diameter of the line to which it was conected.

An analytical approach for sizing the orifice diameters was difficult because of crossflow between control ports of the comparator amplifiers. The signal line size of 0.125 inch (0.318 cm) was chosen on the basis of acceptably low frictional pressure losses. The upstream orifice diameter to terminate this line was empirically determined by feeding pulses to the beginning of the orifice-line combination and observing the pressures delivered to the sensor inputs. Once the average orifice size was determined, the individual orifice sizes were altered to make the sensor yield correct output patterns with the inlet wall pressure distribution of figure 1. The final distribution of signal line orifice sizes obtained by this method is given in table I of the main text.

Internal to the sensor, it was possible to size the interconnecting lines analytically using the procedures outlined in reference 5. Single reflection termination was used since it yielded lines which had low frictional pressure drops and which were close to commercially available tubing sizes. An average interconnecting line size of 0.125 inch (0.318 cm) was used. Graphical techniques were employed to obtain the sensor's internal line sizes. Typical pressure-flow characteristics used in these graphical constructions are given in figures 17 to 21. These characteristics were of the Corning OR-NOR units. The termination characteristics were determined by coupling single

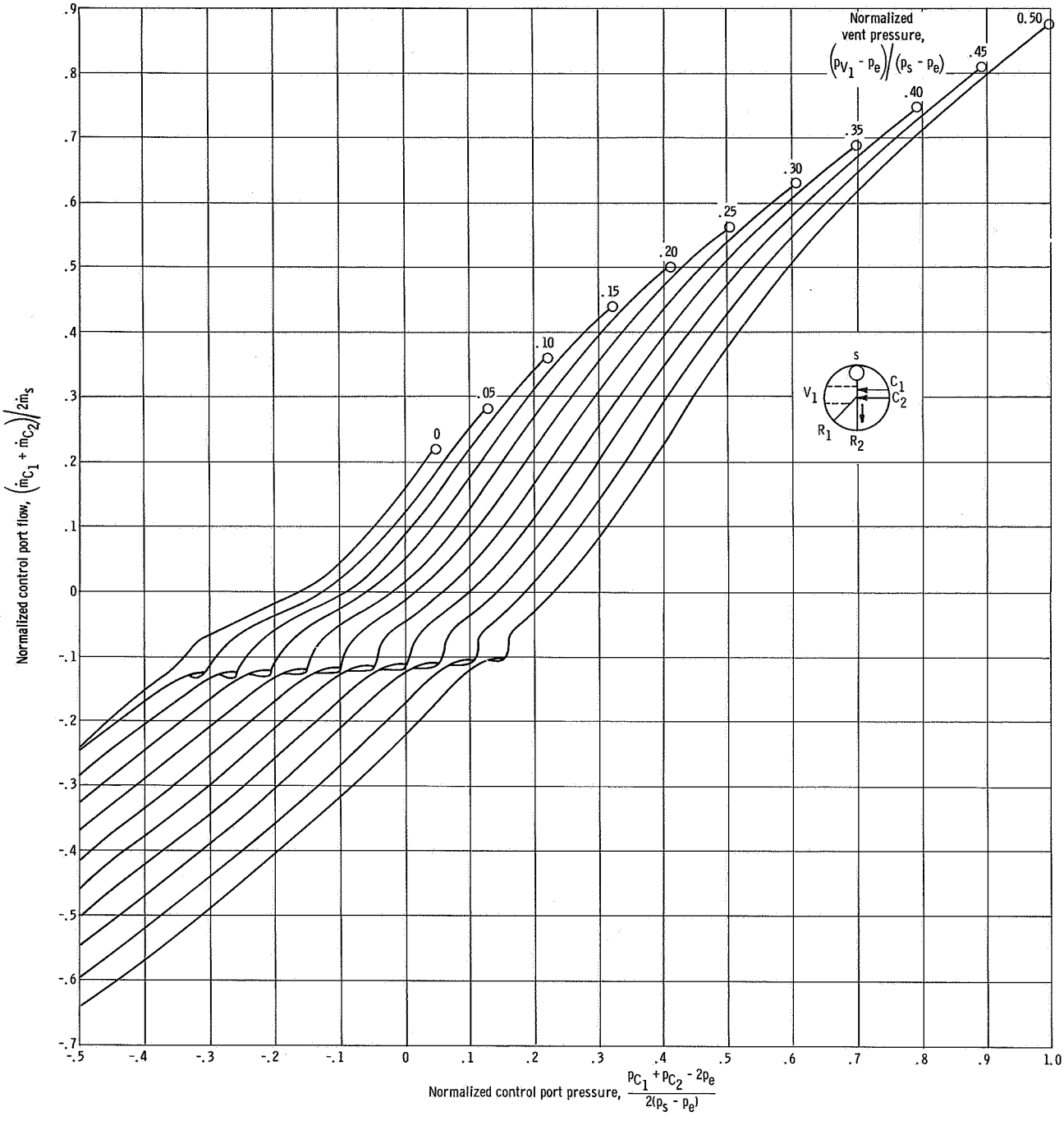

(a) Jet directed to receiver R_2.

Figure 17. - Combined pressure flow characteristics for control ports C_1 and C_2. (Data taken on 2X OR-NOR unit similar to that shown in figure 5.)

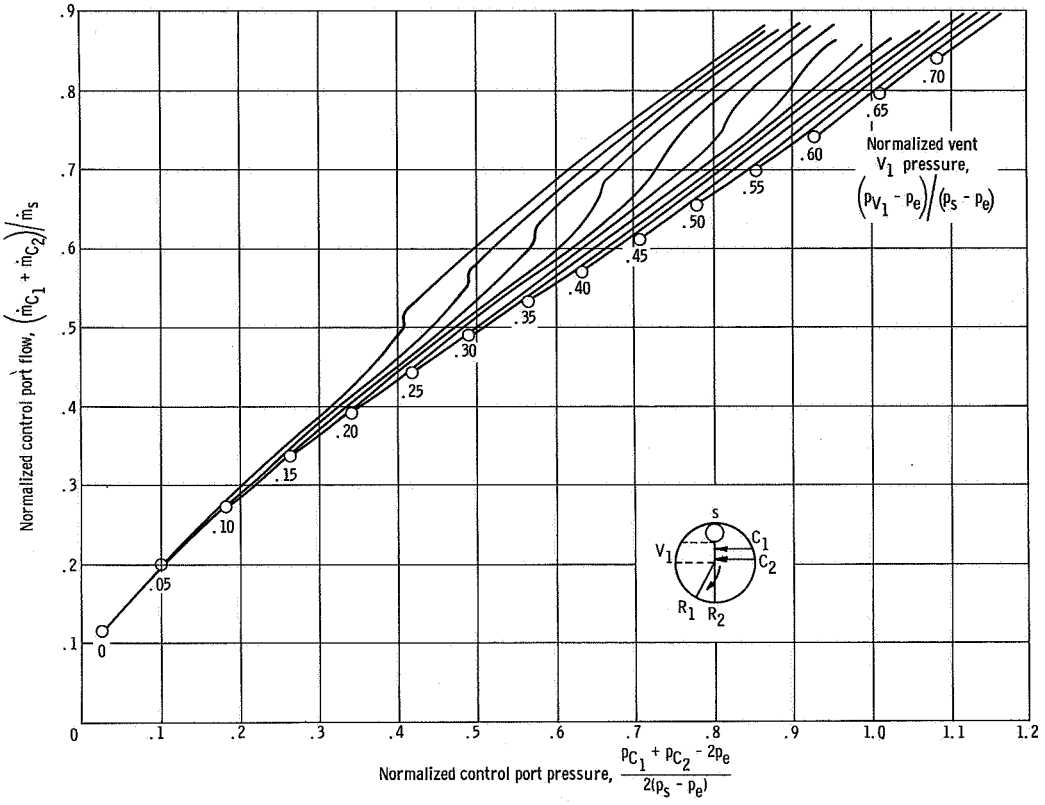

(b) Jet directed to receiver R_1.

Figure 17. - Concluded.

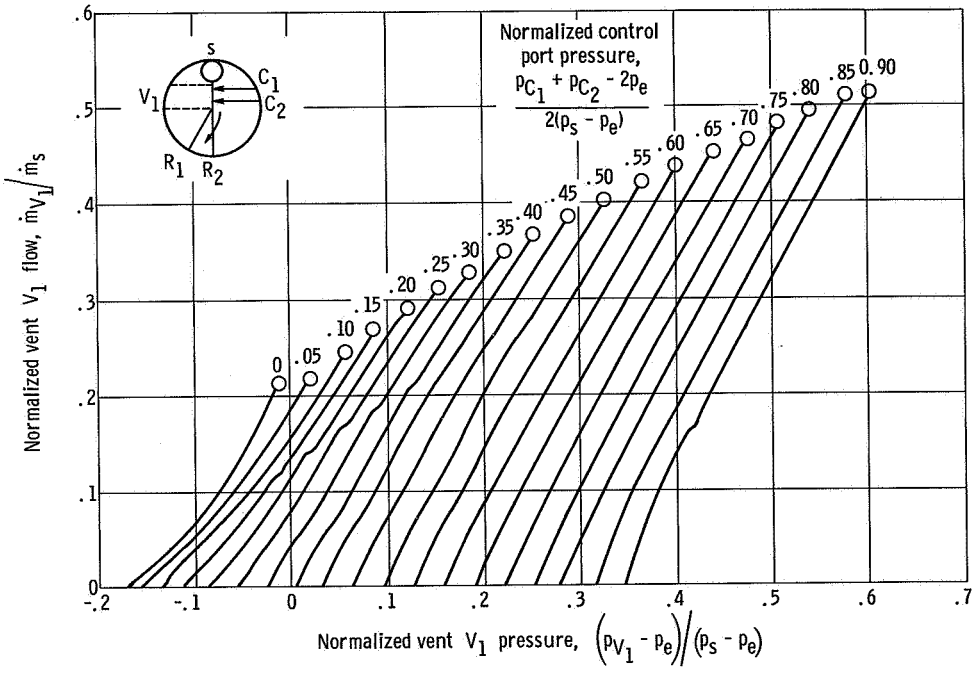

(a) Jet directed to receiver R_1.

Figure 18. - Vent V_1 pressure flow characteristics. (Data taken on 2X OR-NOR unit similar to that shown in figure 5.)

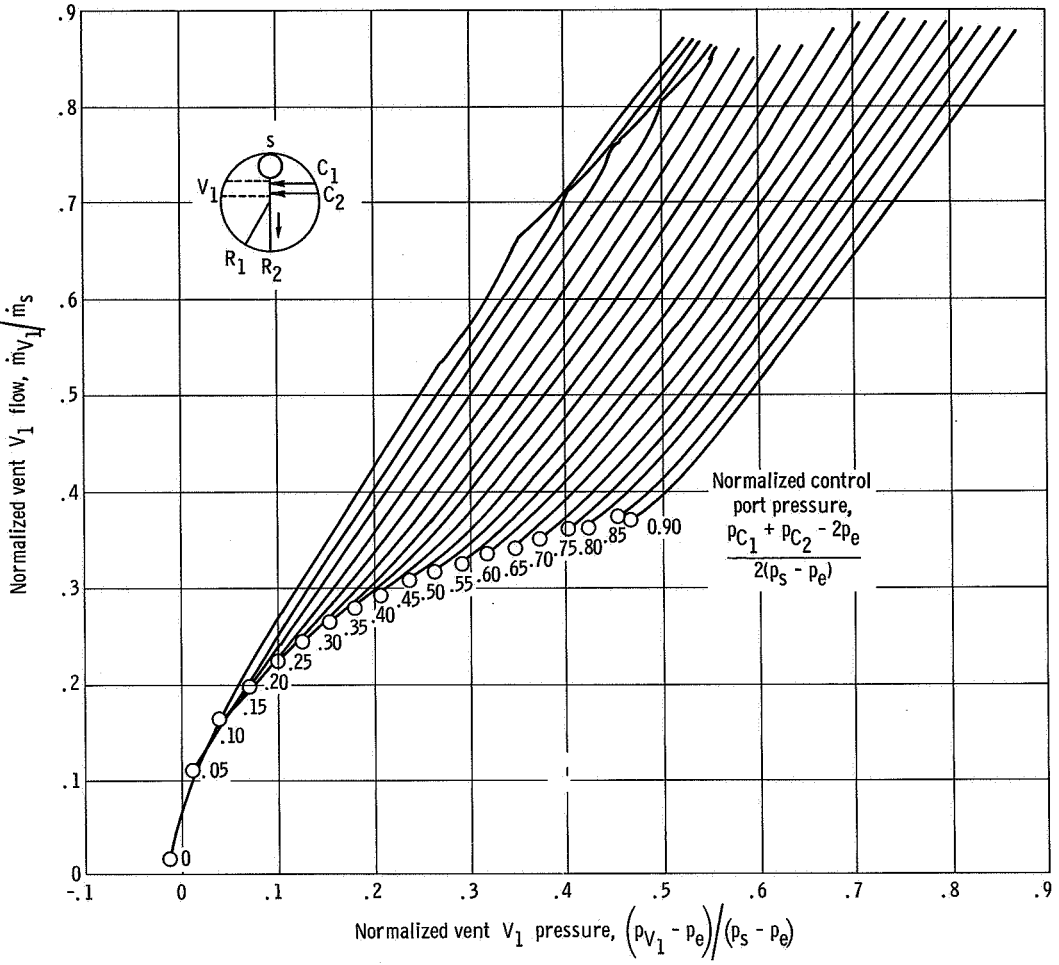

(b) Jet directed to receiver R_2.

Figure 18. - Concluded.

elements with plastic tubing of the closest proper inside diameter. Good agreement was found between observed and predicted pulse heights and waveforms. In some cases, termination was not perfect and reflections occurred (due to the use of a commercially available tubing size rather than the one analytically determined). The magnitude of these reflections, however, was small and did not interfere with proper operation of the circuit.

As mentioned in the text, the prototype shock position sensor worked well before the exhaust manifolds were attached and worked poorly after the manifolds were in place. Obviously, the effects of varying exhaust pressure had deteriorated the performance of some of the sensor's component fluid amplifiers. The remainder of this appendix is devoted to analyzing some of the problem areas which are believed to have caused the shock position sensor's dynamic sensitivity to changing exhaust pressure.

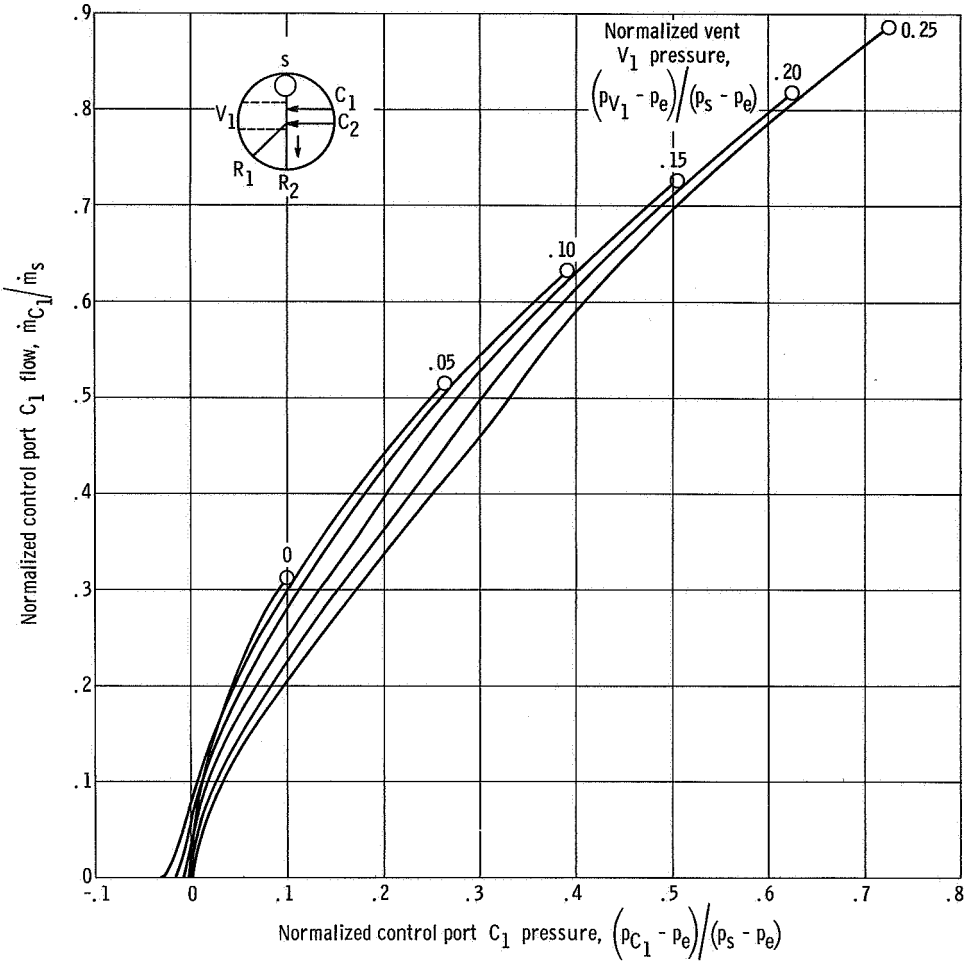

(a) Jet directed to receiver R_2.

Figure 19. - Pressure flow characteristics for control port C_1 with control port C_2 vented to exhaust. (Data taken on 2X OR-NOR unit similar to that shown in figure 5.)

Analysis of Sensor Interconnection Problem Areas

It is believed that most of the dynamic interconnection problems encountered in the prototype shock position sensor can be traced to the switching characteristics of the OR-NOR units. In particular, the unit's sensitivity to positive control port pressures and/or negative vent V_1 pressures when switching from receiver R_1 to receiver R_2 is believed to be responsible. This switching sensitivity is readily seen in the control port pressure-flow characteristics. Figures 17(b), 19(b), and 20(b) show that an average positive control port pressure of only 2 to 3 percent of the amplifier's gage supply

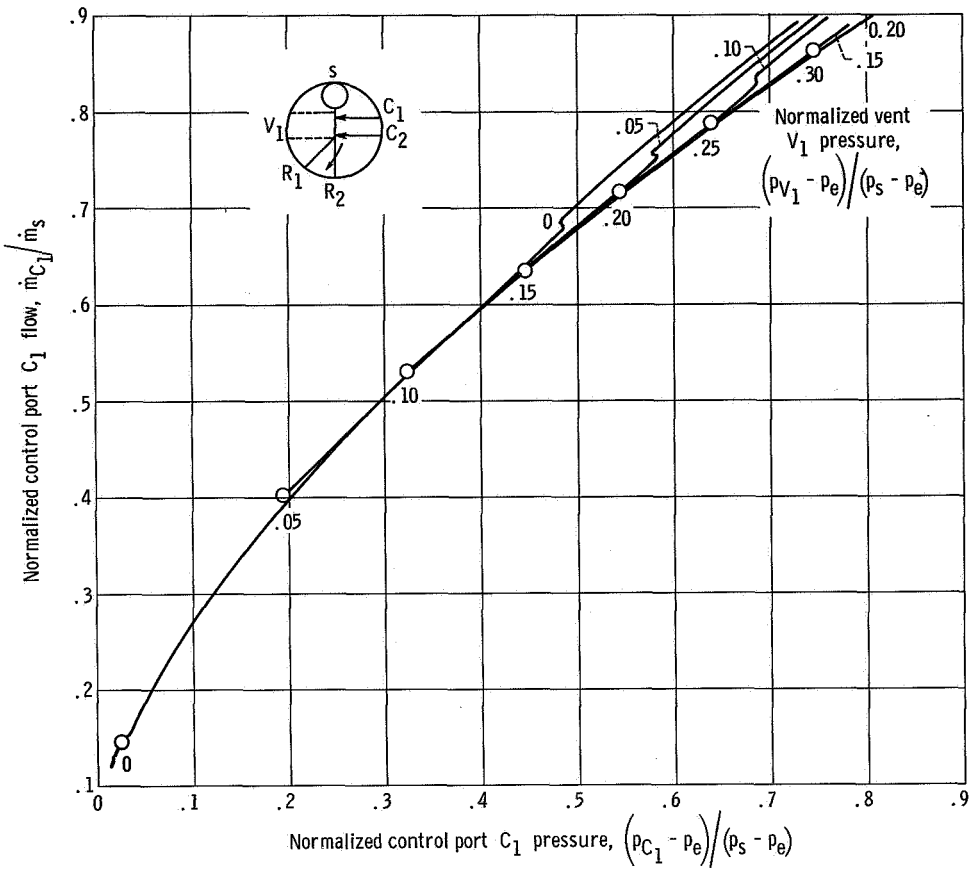

(b) Jet directed to receiver R_1.

Figure 19. - Concluded.

pressure will prevent it from switching from receiver R_1 to reciever R_2 if the vent V_1 pressure is equal to amplifier exhaust. Similarly, figure 18(b) shows that a negative vent V_1 pressure of only 2 percent of supply will keep the amplifier from switching to receiver R_2 when the average control port gage pressure is zero. Static pressure drops much larger than these small values were present in the exhaust manifold. To the exhaust manifold static pressure drops were added the pressures of waves in the exhaust manifolds as comparator or output amplifiers changed state. Thus, ample opportunity existed for cross coupling between various elements in the shock position sensor.

A second possible cause of the sensor's deteriorated performance was the fact that the passive AND units were marginally capable of driving the output amplifiers. When the prototype sensor was first designed, the pressure actuated switches used for sensor readout required actuating pressures approximately 20 percent of the comparator units' supply pressure. The supply pressure to the output stage was maintained at the same value as comparator's supply pressure to provide output pressures capable of actuating

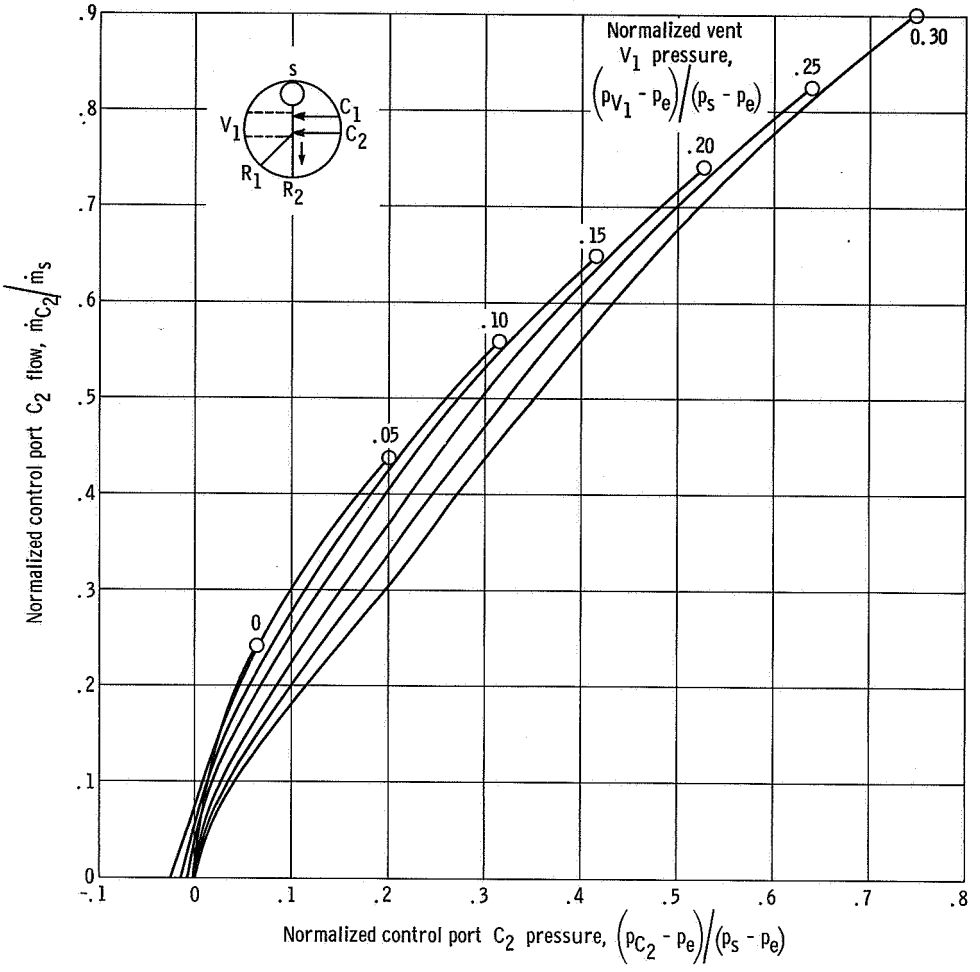

(a) Jet directed to receiver R_2.

Figure 20. - Pressure flow characteristics for control port C_2. Control port C_1 vented to atmosphere. (Data taken on 2X OR-NOR unit similar to that shown in figure 8.)

the switches. Because of the total pressure losses in the passive AND units, their output pressure was calculated to be only 14.5 percent of output unit supply pressure. The data of figure 19(a) shows that OR-NOR units require control pressures of only 10 percent of supply to switch. Thus, this driving pressure should be sufficient if component variations and receiver loading effects do not have to be taken into account. Unfortunately, however, substantial variations in switching pressures exist between various OR-NOR units. In addition, OR-NOR units become more difficult to switch into the R_1 receiver if the R_1 receiver is driving a load such as an orifice or the control port of another amplifier.

If the gage supply pressure to the output units is reduced by a factor of two (corresponding to a throat Mach number of 0.675 instead of the previous value of 0.905 calcu-

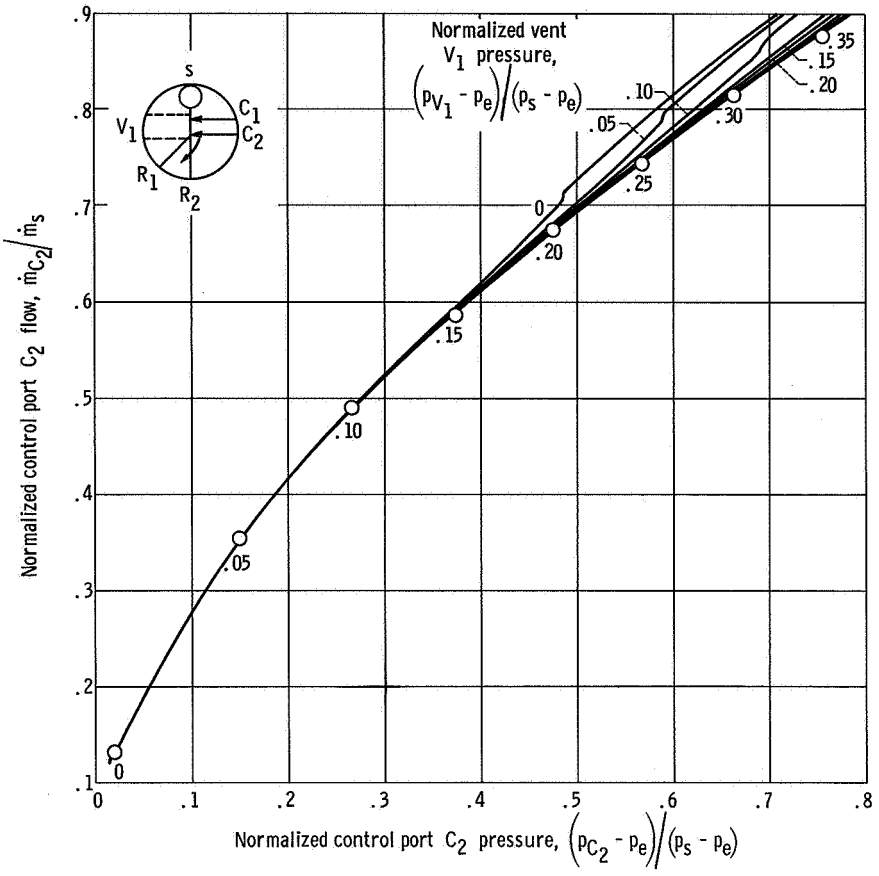

(b) Jet directed to receiver R_1.

Figure 20. - Concluded.

lated in appendix A), then the logical AND units are able to furnish a signal pressure of 30 percent of the output units' supply, an adequate amount for driving the control ports of the output unit. Such a reduction in the supply pressure to the output units is considered permissible since a second set of pressure actuated switches was obtained which would switch on less than 1 inch of water (0.025 N/cm^2). Under wind tunnel conditions, the pressures delivered to the switches would be 1.2 psig (0.827 N/cm^2) a value far higher than their actuating pressure.

A third, final cause of sensor deteriorated performance could lie in the passive AND unit. Supply pressures to the power nozzles of the OR-NOR units which comprise the passive AND units is only 38 percent of the gage supply pressure to the comparator units. Thus, from figure 17(b), it is seen that vent pressures of only 2 percent $\times$ 0.38 or 0.76 percent of the comparator unit's gage supply pressure will keep the passive AND units from returning to their NOR leg outputs in the absence of control port pressures. This value is a very small percentage of the comparator's supply pressure and

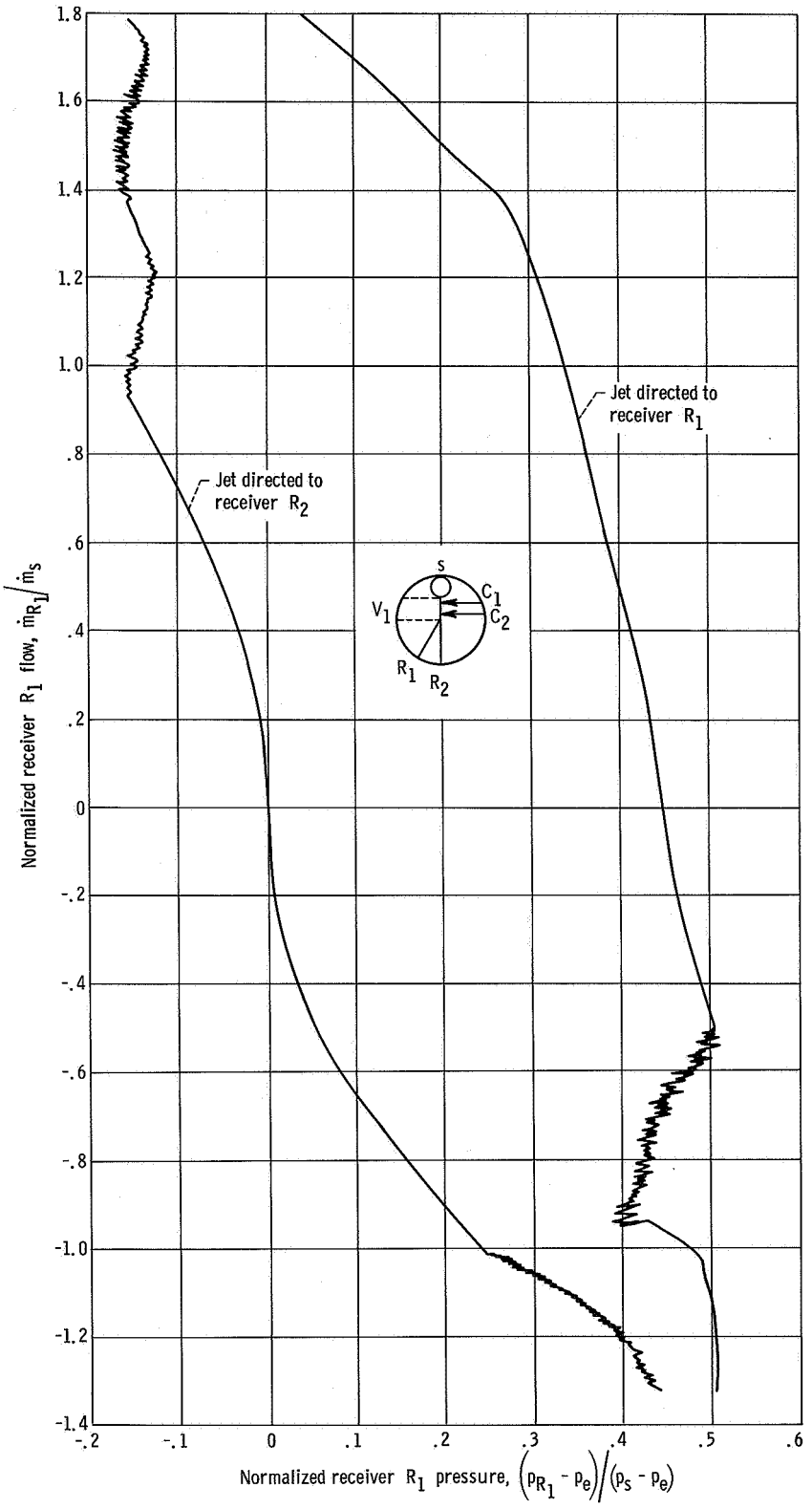

(a) Receiver R_1 characteristics. Receiver R_2 vented to exhaust.

Figure 21. - Receiver pressure flow characteristics. (Data taken on 2X OR-NOR unit similar to that shown in figure 5.)

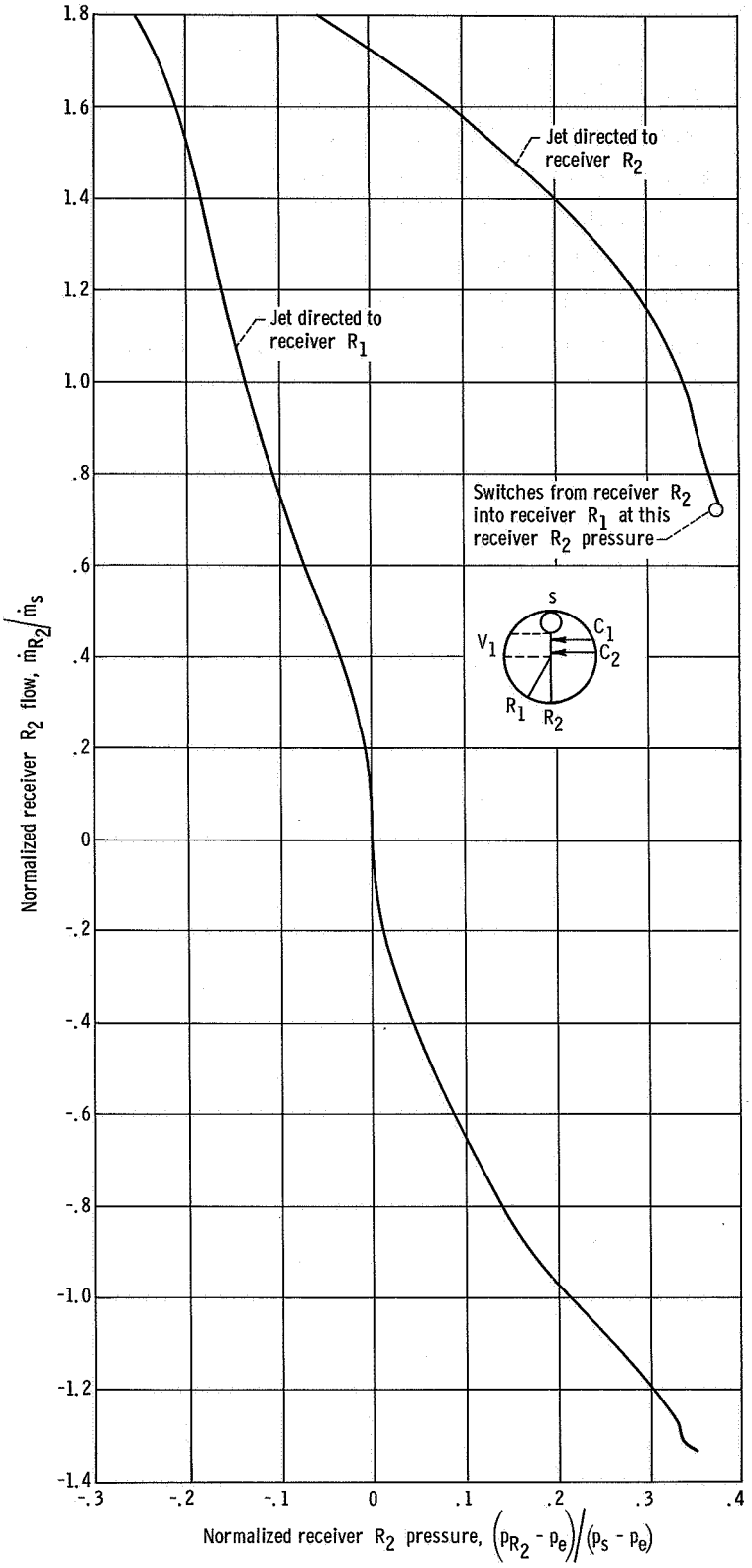

(b) Receiver R_2 characteristics. Receiver R_1 vented to exhaust.

Figure 21. - Concluded.

could easily occur as a result of small waves in the exhaust ducting or, for that matter, as a result of frictional and turning losses in the exhaust ducting. Laboratory bench tests with the exhaust manifolds removed did not indicate the sensor's operational problems which were encountered when the manifolds were installed. Thus, further improvements to the shock position sensor should include the following:

(1) Enlargement of the exhaust manifold cross-sectional flow areas so that pressure drops in them are negligible

(2) Use of an OR-NOR unit in the passive AND stage which does not have the reverse switching sensitivity to vent V_1 pressures that the present OR-NOR units have

APPENDIX C

SYMBOLS

A, B, C, D, E, F	static wall pressure taps on the inlet's wall (also refers to pressures measured by these taps)
	Boolean logical AND function (has value of true only if two inputs to the AND function have the value of logical true)
c_j	speed of sound in power nozzle of fluid jet amplifier
C_1, C_2	control ports on fluid jet amplifier
D_j	width of power nozzle of fluid jet amplifier, in.; cm
k	ratio of specific heats of air
g_o	acceleration of gravity, (lb mass)(in.)/(lb force)(sec^2); (kg)(cm)/(N)(sec^2)
M	Mach number
M_{max}	maximum Mach number at which fluid jet amplifier will operate
$\dot{m}$	mass flow rate
p	pressure, psi; N/cm^2
R_1, R_2	receiver of fluid jet amplifier
Re_{min}	minimum Reynolds number at which fluid jet amplifier will operate
S_{XY}	outputs of logical AND units of shock position sensor, indicate a possible shock location between pressure taps X and Y
S'_{XY}	outputs of logical eqs. (2) (indicate exclusive existence of a shock location between pressure taps X and Y)
S''_{XY}	outputs of logical eqs. (3), (also shock position sensor) (indicate non-exclusive existence of a shock between stations X and Y - i.e., existence of S''_{XY} means that either a shock exists between stations X or Y or that the output S''_{YZ} or higher exists)
T	temperature, ^oR; K
V_1	interaction region vent of fluid jet amplifier
OR	Boolean logical OR function (has the value true if either of the two inputs to it has the value true)

NOR	Boolean logical NOR function (has the value true only if neither of the two inputs to it has the value true)
ρ	density, lb mass/in^3; kg/cm^3
μ	viscosity, lb force (sec)/(in.^{2}); N (sec)/cm^2

Subscripts:

A, B, C, D, E, F	refers to the pressure taps A, B, C, D, E, F, respectively
C_1, C_2	respective control ports of fluid jet amplifier
e	refers to amplifier exhaust conditions
j	refers to conditions at throat of amplifier power nozzle or to sensor exhaust pressure
s	refers to supply conditions to fluid jet amplifiers or to sensor supply conditions
th	throat conditions in supersonic inlet, ahead of normal shock wave
V_1	interaction region vent of fluid jet amplifier
min	minimum value
max	maximum value

Superscript:

$\overline{\quad}$	denotes logical complement of quantity

REFERENCES

1. Cubbison, R. W. ; Meleason, E. T. ; and Johnson, D. F. : Effect of Porous Bleed in a High-Performance Axisymmetric, Mixed-Compression Inlet at Mach 2. 50. NASA TM X-1692, 1968.

2. Gilbertson, R. O. : Fluerics Terminology, Nomenclature, and Schematics. Rep. NOTS TP 4231, Naval Ordnance Test Station Feb. 1967.

3. Griffin, William S. : A Breadboard Flueric - Controlled Pneumatic Stepping-Motor System. NASA TN D-4495, 1968.

4. Greber, Isaac; Taft, Charles; and Abler, Joseph: Experimental Scaling Study of Fluid Amplifier Elements. Case Inst. Tech. (NASA CR-75668), Mar. 31, 1966.

5. Kirshner, Joseph M. : Fluid Amplifiers, McGraw-Hill Book Co., Inc., 1966.

6. Bowditch, David N. ; and Anderson, Bernhard H. : Investigation of the Performance and Control of a Mach 3. 0, Two Dimensional, External-Internal-Compression Inlet. NASA TM X-470, 1961.

7. Bowditch, David N. ; Anderson, Bernhard H. ; and Tabata, William K. : Performance and Control of a Full-Scale, Axially Symmetric, External-Internal-Compression Inlet from Mach 2. 0 to 3. 0. NASA TM X-471, 1961.

"The aeronautical and space activities of the United States shall be conducted so as to contribute . . . to the expansion of human knowledge of phenomena in the atmosphere and space. The Administration shall provide for the widest practicable and appropriate dissemination of information concerning its activities and the results thereof."

—NATIONAL AERONAUTICS AND SPACE ACT OF 1958

NASA SCIENTIFIC AND TECHNICAL PUBLICATIONS

TECHNICAL REPORTS: Scientific and technical information considered important, complete, and a lasting contribution to existing knowledge.

TECHNICAL NOTES: Information less broad in scope but nevertheless of importance as a contribution to existing knowledge.

TECHNICAL MEMORANDUMS: Information receiving limited distribution because of preliminary data, security classification, or other reasons.

CONTRACTOR REPORTS: Scientific and technical information generated under a NASA contract or grant and considered an important contribution to existing knowledge.

TECHNICAL TRANSLATIONS: Information published in a foreign language considered to merit NASA distribution in English.

SPECIAL PUBLICATIONS: Information derived from or of value to NASA activities. Publications include conference proceedings, monographs, data compilations, handbooks, sourcebooks, and special bibliographies.

TECHNOLOGY UTILIZATION PUBLICATIONS: Information on technology used by NASA that may be of particular interest in commercial and other non-aerospace applications. Publications include Tech Briefs, Technology Utilization Reports and Notes, and Technology Surveys.

Details on the availability of these publications may be obtained from:

SCIENTIFIC AND TECHNICAL INFORMATION DIVISION

NATIONAL AERONAUTICS AND SPACE ADMINISTRATION

Washington, D.C. 20546